

Mechanistic insights into actin-driven polarity site movement in yeast

Debraj Ghose^{a,b} and Daniel Lew^{b,*}

^aComputational Biology and Bioinformatics and ^bDepartment of Pharmacology and Cancer Biology, Duke University Medical Center, Durham, NC 27710

ABSTRACT Directed cell growth or migration are critical for the development and function of many eukaryotic cells. These cells develop a dynamic “front” (also called “polarity site”) that can change direction. Polarity establishment involves autocatalytic accumulation of polarity regulators, including the conserved Rho-family GTPase Cdc42, but the mechanisms underlying polarity reorientation remain poorly understood. The tractable model yeast, *Saccharomyces cerevisiae*, relocates its polarity site when searching for mating partners. Relocation requires polymerized actin, and is thought to involve actin-mediated vesicle traffic to the polarity site. In this study, we provide a quantitative characterization of spontaneous polarity site movement as a search process and use a mechanistic computational model that combines polarity protein biochemical interactions with vesicle trafficking to probe how various processes might affect polarity site movement. Our findings identify two previously documented features of yeast vesicle traffic as being particularly relevant to such movement: tight spatial focusing of exocytosis enhances the directional persistence of movement, and association of Cdc42-directed GTPase-Activating Proteins with secretory vesicles increases the distance moved. Furthermore, we suggest that variation in the rate of exocytosis beyond simple Poisson dynamics may be needed to fully account for the characteristics of polarity site movement in vivo.

Monitoring Editor

Leah Edelstein-Keshet
University of British Columbia

Received: Jan 15, 2020

Revised: Mar 2, 2020

Accepted: Mar 10, 2020

INTRODUCTION

Cell polarity is critical to the function of almost all cells. For many cells, it is also vital to dynamically alter the direction of polarity. For instance, migratory cells form a polarized front that reorients (turns) in response to changing external signals (Iglesias and Devreotes, 2008; Graziano and Weiner, 2014). Similarly, the polarized tips of hyphal fungi, plant root hairs, neuronal axons, and pollen tubes grow and change direction in response to chemical or physical cues (Hoch *et al.*, 1987; Palanivelu and Preuss, 2000; von Philipsborn and Bastmeyer, 2007; Hong and Nishiyama, 2010;

Nakamura and Grebe, 2018). Yeast possess dynamically changing polarity sites too. For instance, germinating fission yeast spores have a polarity site that appears to wander around the cortex before stabilizing to promote outgrowth (Bonazzi *et al.*, 2014). Haploid budding yeast cells also display a wandering polarity site in the context of mating (Dyer *et al.*, 2013; Hegemann *et al.*, 2015; McClure *et al.*, 2015). The mechanisms dictating polarity site relocation are poorly understood.

The molecular mechanisms that establish cell polarity are conserved across eukaryotes and involve Rho-family GTPases (Cdc42 in yeast and mammals) (Etienne-Manneville, 2004; Park and Bi, 2007). GTP-Cdc42 becomes concentrated in a cortical region that determines the cell's front, and this polarized domain is built and maintained by autocatalytic positive feedback (Johnson *et al.*, 2011; Chiou *et al.*, 2018). However, the location of the front is subject to change in response to either external cues (as mentioned above) or intrinsic factors (Ozbudak *et al.*, 2005; Artemenko *et al.*, 2014; Bonazzi *et al.*, 2014; Graziano and Weiner, 2014; McClure *et al.*, 2015). Polarity proteins exchange rapidly between membrane and cytoplasm (Wedlich-Soldner *et al.*, 2004; Dyer *et al.*, 2013). Thus, relocation of polarity does not reflect a physical displacement of those

This article was published online ahead of print in MBoC in Press (<http://www.molbiolcell.org/cgi/doi/10.1091/mbc.E20-01-0040>) on March 18, 2020.

*Address correspondence to: Daniel Lew (daniel.lew@duke.edu).

Abbreviations used: CDF, cumulative density function; GAP, GTPase-activating protein; GDI, guanine nucleotide dissociation inhibitor; GEF, guanine nucleotide exchange factor; GPCR, G-protein coupled receptors; MAPK, mitogen-activated protein kinase; PAK, p21-activated kinase.

© 2020 Ghose and Lew. This article is distributed by The American Society for Cell Biology under license from the author(s). Two months after publication it is available to the public under an Attribution–Noncommercial–Share Alike 3.0 Unported Creative Commons License (<http://creativecommons.org/licenses/by-nc-sa/3.0>).

“ASCB®,” “The American Society for Cell Biology®,” and “Molecular Biology of the Cell®” are registered trademarks of The American Society for Cell Biology.

proteins along the membrane, but rather a change in the location of the centroid of the cluster or patch of polarity proteins at the membrane. The dynamical relocation of the polarity patch has been suggested to arise from either of two conceptually distinct types of mechanisms. First, the effect of molecular noise in a system with weak (linear) positive feedback can cause stochastic relocation of the polarity patch (Jilkine *et al.*, 2011; Hegemann *et al.*, 2015). Because positive feedback tends to stabilize the position of the polarity patch, molecular noise would have a weaker impact on systems with strong positive feedback. However, addition of a localized negative feedback to a system with strong (nonlinear) positive feedback can lead to wavelike propagation of the polarity patch and make its location responsive to external stimuli (Meinhardt, 1999; Ozbudak *et al.*, 2005; Dyer *et al.*, 2013; Graziano and Weiner, 2014; McClure *et al.*, 2015; Devreotes *et al.*, 2017). We note that these mechanisms are not mutually exclusive, and that the movement of the yeast polarity patch is not purely wavelike: a combination of brief periods of wavelike movement interrupted by stochastic events that reorient the movement may yield a fuller description than either purely noise-driven or purely wavelike movement.

Many signaling pathways display negative feedback loops, which can promote adaptation and homeostasis as well as oscillations in regulatory networks (Brandman and Meyer, 2008). In the context of moving polarity sites, negative feedback has been proposed to operate via Arp2/3-nucleated branched actin networks (in neutrophils) or formin-nucleated linear actin cables (in yeast) to regulate upstream GTPases Rac and Cdc42 (Dyer *et al.*, 2013; Graziano and Weiner, 2014; McClure *et al.*, 2015).

Here we focus on the mechanism of polarity patch movement in mating cells of the yeast *Saccharomyces cerevisiae*. Haploid yeast cells (which exist as α or a mating types) signal to each other by secreting pheromones. G-protein coupled receptors (GPCRs) bind to pheromone from cells of the opposite mating type and activate a mitogen-activated protein kinase (MAPK) cascade (Pryciak and Huntress, 1998). MAPK activation leads to cell cycle arrest in G1, transcription of mating-related genes, and Cdc42 polarization. The location of polarization is influenced both by the spatial gradient of pheromone, which acts through the GPCRs to influence local Cdc42 activation, and by internal landmark proteins, which act via the Rap1-family GTPase Rsr1 to influence Cdc42 (Madden and Snyder, 1992; Butty *et al.*, 1998; Nern and Arkowitz, 1998; Nern and Arkowitz, 1999). Mating cells can polarize directly toward a nearby partner, but they frequently polarize in a different direction and then relocate the polarity patch to the correct location (Hegemann *et al.*, 2015; Henderson *et al.*, 2019; Wang *et al.*, 2019).

Polarization can also occur at a random location when the spatial cues that normally guide polarization are eliminated (e.g., by artificially activating the MAPK without pheromone in cells lacking *RSR1*) (Strickfaden and Pryciak, 2008; McClure *et al.*, 2015). In the absence of pheromone from partner cells, the polarity patch wanders spontaneously around the cell cortex. This finding demonstrates that movement of the polarity patch does not require a pheromone gradient and provides the opportunity to study undirected polarity patch movement.

Previous findings indicated that movement was greatly reduced on actin depolymerization (Dyer *et al.*, 2013; Hegemann *et al.*, 2015; McClure *et al.*, 2015), suggesting that F-actin somehow drives the relocation of the polarity patch. There are two main roles of F-actin in mating yeast: linear bundles called actin cables deliver cargo including secretory vesicles to the polarity site, and branched structures called actin patches promote endocytosis at the plasma membrane. Computational modeling of the biochemistry of Cdc42

polarization provided considerable insight into how this system breaks symmetry and guarantees a single polarity axis (Otsuji *et al.*, 2007; Goryachev and Pokhilko, 2008; Mori *et al.*, 2008; Howell *et al.*, 2009; Wu *et al.*, 2015; Chiou *et al.*, 2018). Addition of vesicle trafficking (exocytosis and endocytosis) to the model revealed that vesicles have the capacity to perturb polarity (Layton *et al.*, 2011; Savage *et al.*, 2012), potentially causing movement of the polarity patch (Dyer *et al.*, 2013; McClure *et al.*, 2015). However, it is unclear to what extent the polarity patch movement observed *in vivo* can be explained by the effects of vesicle traffic.

Here we examine the undirected movement of polarity patches *in vivo*, deriving quantitative measures that characterize the magnitude and directional persistence of the movement. We also examine the requirements for patch movement in a computational model that combines polarity factor biochemistry and vesicle trafficking. We find that patch movement *in silico* is driven by exocytosis and not endocytosis. It relies on the fact that secretory vesicles insert membrane that locally dilutes polarity factors and would not occur if secretory vesicles were to concentrate polarity factors. Analysis of the model suggested that a combination of three factors must be considered to account for the quantitative aspects of patch movement. First, to generate sufficiently persistent motion, vesicle delivery must be focused to a narrow zone that occupies only part of the polarity site, as observed in cells (Lawson *et al.*, 2013; McClure *et al.*, 2015). Second, to generate a movement magnitude comparable to that in cells, vesicles must deliver some polarity antagonist, like Cdc42-directed GTPase-activating proteins (GAPs), as is thought to occur in yeast (Ozbudak *et al.*, 2005; Knaus *et al.*, 2007; Mukherjee *et al.*, 2013). Third, to reproduce the variability of patch movement we observed *in vivo*, there must be some variation in the rate of vesicle delivery, suggesting that exocytosis events may occur in bursts. Our findings indicate that incorporating focused and temporally variable vesicle-mediated GAP delivery can lead to a quantitative match between polarity site movement in cells and in a computational model. Thus, these features are in principle sufficient to explain polarity site movement in yeast.

RESULTS

Characterization of undirected polarity patch movement

Our experimental system to investigate the mechanism of undirected polarity patch movement in budding yeast consists of haploid *rsr1 Δ* cells induced to artificially activate the pheromone-responsive MAPK pathway in the absence of pheromone by inducing a membrane-anchored version of the MAPK scaffold Ste5 (Pryciak and Huntress, 1998; McClure *et al.*, 2015). Previous studies analyzed patch mobility by measuring the patch's mean squared displacement over time (Dyer *et al.*, 2013; McClure *et al.*, 2015), but we sought to characterize patch movement in greater detail. To this end, we imaged populations of cells taking confocal z-stacks at 1.5-min intervals (snapshots from a movie of a cell are shown in Figure 1A) and calculated the 3D position of the centroid of the patch at each time point to generate tracks that consisted of a series of movement vectors (Figure 1B; see *Materials and Methods* for details). From each vector, we extracted 1) its magnitude or "step length" and 2) its angle with respect to the preceding vector, or "turning angle." Distributions of these two metrics are shown in Figure 1, C–E. To assess how reproducible these patch mobility characteristics were, we compared a dataset reported previously (McClure *et al.*, 2015) with a newer dataset reported in this study. As shown in Supplemental Figure S1, A–C, movement metric distributions were highly reproducible, suggesting that patch movement is a robust phenomenon despite variation in experimental conditions.

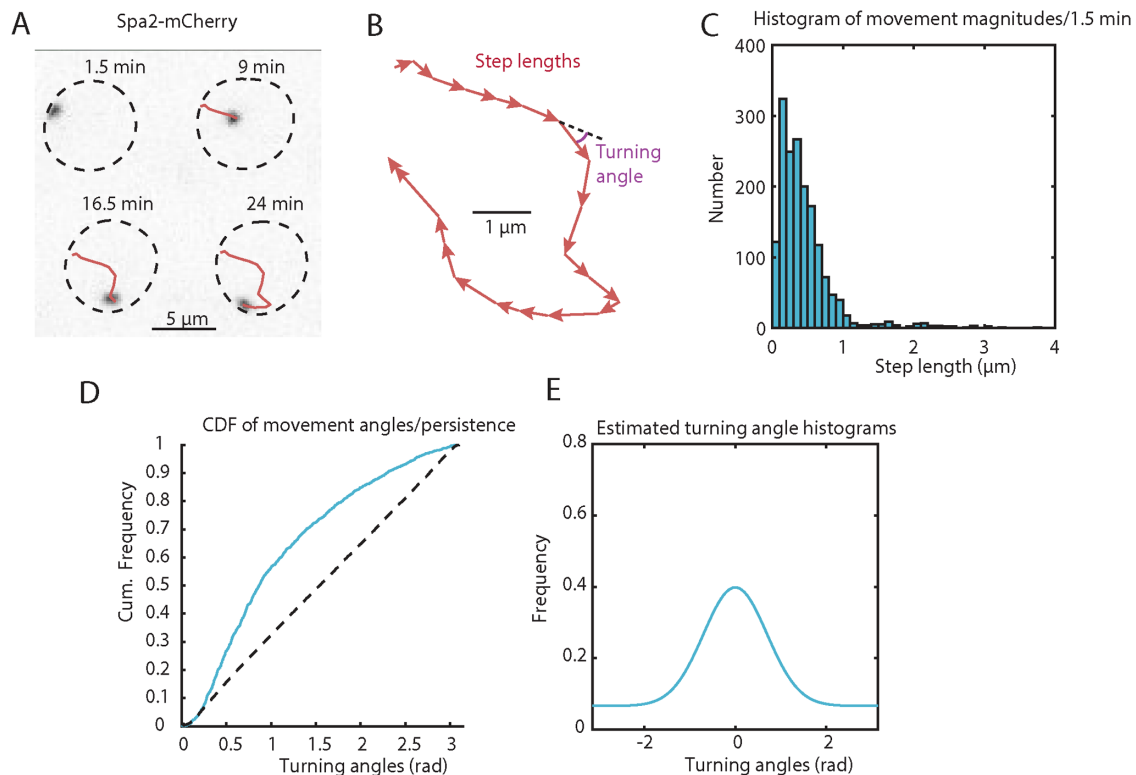


FIGURE 1: Characteristics of in vivo patch movement. (A) Selected snapshots from time-lapse imaging of a moving polarity patch in a yeast cell harboring Spa2-GFP (DLY18172) and induced to activate the mating pathway in the absence of pheromone. Inverted maximum projections of 15 z-plane images. Dashed line, cell outline. Red line traces path of the centroid of the moving patch. (B) Trace from centroid positions of the patch in cell from A taken at 1.5-min intervals, represented as a series of movement vectors, where each movement vector has a magnitude (step length) and turning angle. (C) Histogram of step lengths, derived from $N = 1701$ steps from cells treated and imaged as in A. (D) Cumulative frequency plot of turning angles from the same cells. Dashed line is expected cumulative frequency if turning angles were sampled from a uniform distribution. (E) Estimated histogram of planar turning angles on the surface a sphere with radius $2.5\ \mu\text{m}$ that would yield the cumulative distribution of 3D angles plotted in D (see *Materials and Methods*).

It is evident from the histogram for step lengths in Figure 1C that the distances moved by the patch in each 1.5-min interval vary considerably, yielding a skewed (non-normal) distribution with a long tail of large step lengths. To analyze the distribution of turning angles, we needed to convert our measured distribution of 3D angles into a planar angle distribution, because polarity patches actually move along a 2D cell surface, not a 3D space. We began by plotting the cumulative density function (CDF) of the measured 3D angles (Figure 1D). The black dashed line indicates the CDF to be expected for a uniform distribution of turning angles, and the observed deviation from this uniform distribution indicates that patches tend to continue moving in the same general direction (i.e., show a preference for smaller turning angles). A similar persistence of motion was noted in other experimental settings (Ozbudak *et al.*, 2005; Dyer *et al.*, 2013). To extract the distribution of planar turning angles that might have yielded this CDF, we ran simulations of moving patches on the surface of $5\text{-}\mu\text{m}$ diameter spheres. We found that the experimentally observed distribution of turning angles could be phenomenologically described by the function $e^{-\frac{(\theta)^2}{2 \times \sigma^2} + k}$, which is a Gaussian shifted along the y-axis by k (where the independent variable is θ , the angle of movement) that accounts for the observed persistence. This “offset Gaussian” distribution (Figure 1E) is centered at 0 radians and its standard deviation (SD) (σ) provides a measure of

the degree of persistent motion—that is, the degree to which the patch will continue to move in a given direction.

Patch movement as a search strategy

We assume that the physiological role of patch movement is to facilitate the search for mating partners. Previous studies of moving agents engaged in search patterns have focused on searching large planar areas for food or prey and highlighted the advantageous properties of Lévy flights in this context (Viswanathan *et al.*, 2008; Humphries and Sims, 2014). Lévy flights are random walks in which the step-size distribution exhibits a heavy tail that decays as a power law. However, a log-log plot of the step-length histogram for yeast polarity patches (Supplemental Figure S2A) revealed that it was not bound by an exponential or power law, but could be approximated by a gamma distribution (Supplemental Figure S2B). Thus, patch movement does not appear to be an example of a Lévy flight. The yeast cell’s search for a partner is somewhat different from the search of a large planar area. Yeast cells themselves are not motile and will only mate if there is a potential partner very close by. Thus, if we consider polarity patch movement as a search process, the successful search is one that brings the two patches in adjacent partner cells to be close to each other. We wished to understand how the observed distributions of step lengths and turning angles impacted the effectiveness of such a partner search.

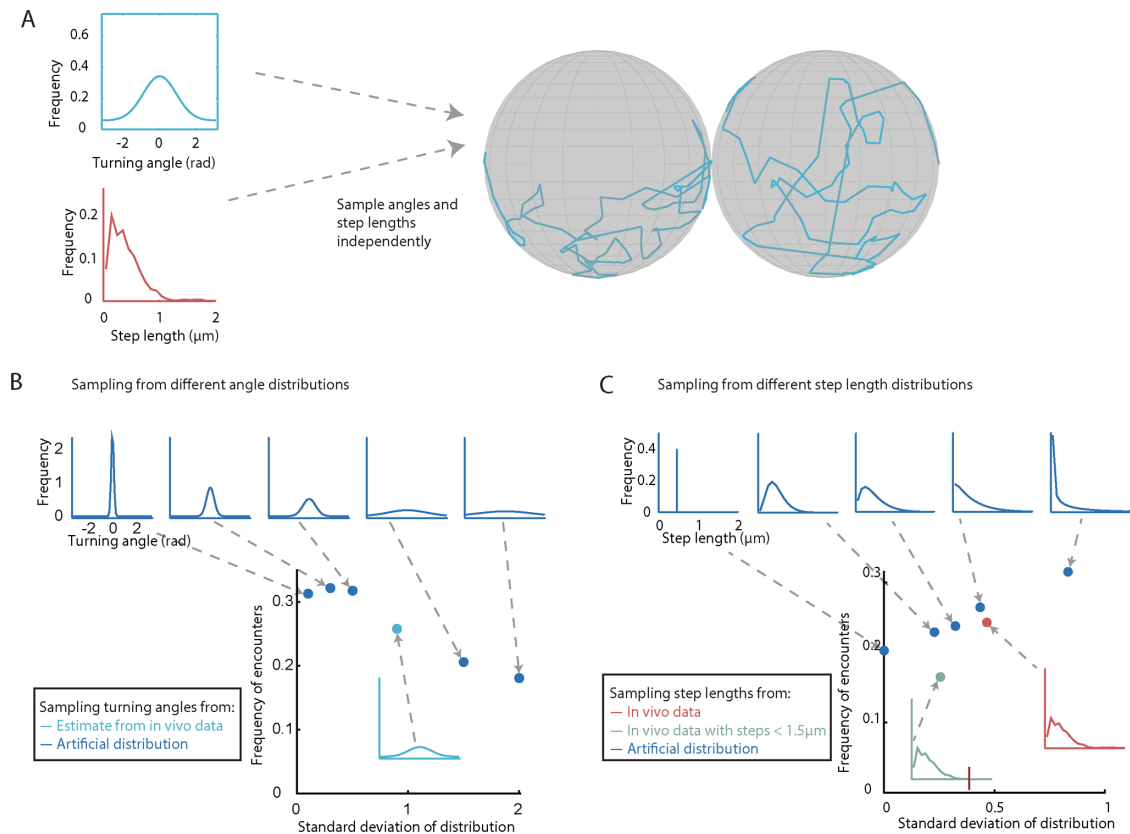


FIGURE 2: Effect of patch movement characteristics on the search for mating partners. (A) Step lengths and turning angles were independently sampled from the distributions in Figure 1 to simulate moving patches on two adjacent spheres with radius 2.5 μm . Simulated particles moved along the surface of the sphere, but for comparison with time-lapse imaging of cells, traces were drawn by linking discrete patch positions (at 1.5-min intervals) with straight lines. (B) Simulations similar to those in A were run by sampling from experimentally determined step lengths but using artificial turning angle distributions with different standard deviations (blue insets). The success of the search process was quantified by plotting the frequency of encounters (fraction of simulations in which pairs of patches got within 2 μm of each other in < 150 min). (C) Simulations similar to those in B were run by sampling from the experimental turning angle distribution but using artificial step length distributions (blue insets).

Recall that when a cell polarizes away from its partner, its patch moves erratically before becoming aligned with the partner's patch. This raised the question of how effectively patches in adjacent cells could come close to each other purely via unguided movement. To address this question, we carried out particle-based simulations. Each simulation consisted of two adjacent spherical cells, where each cell had a particle (representing the patch) moving in a stochastic manner along its surface. The initial condition for each simulation was particles placed randomly on the half of the sphere that faced away from the partner. We then moved each particle along the cell cortex by independently sampling step lengths and angles from experimental data; Figure 2A displays an illustrative example of the particle tracks we obtained. As a measure of successful search, we recorded the fraction of simulations whose patches came within 2 μm of each other within 150 min (a physiologically relevant timescale for mating). This metric was 23–25% for simulations using step length and offset Gaussian turning angle distributions derived from the experimental data (blue dot in Figure 2B and orange dot in Figure 2C).

We then ran simulations where step lengths were sampled from experimental data, but turning angles were sampled from a variety of offset Gaussian distributions with differing standard deviations, as a way to ask how success of the search may depend on the degree of persistence in patch movement. We found that optimal searching

occurred when the Gaussian had a SD of 0.3 rad. The existence of an optimal degree of persistence can be intuitively understood as follows: if patch movement showed no persistence (uniform turning angles), a diffusive search would take a long time for patches that start in a distant location from the partner (as enforced by our initial condition). Persistent motion allows more rapid escape from the local neighborhood, and as persistence increases, the escape probability rises. However, perfect persistence would lead to a patch that travels in a great circle around the sphere and cannot access other parts of the landscape: optimal search requires a combination provided by imperfect persistence. For our data from yeast patches, the estimated SD of the offset Gaussian is 0.9 rad, which is suboptimal from the point of view of the search process. This suggests that mechanistic aspects driving patch movement may constrain the persistence of such movement (Figure 2B). However, we note that the undirected search process characterized here may differ in important ways from a physiological search that is guided by pheromone gradients.

We also ran simulations where, this time, turning angles were sampled from experimental data but step lengths were sampled from artificial probability distributions with the same mean step length (0.456 μm) as the experimental distribution. The first distribution set all steps equal to 0.456 μm (SD $\sigma = 0$; Figure 2C inset, top left). The others are gamma distributions with different shape and scale parameters selected to yield the same mean step length but

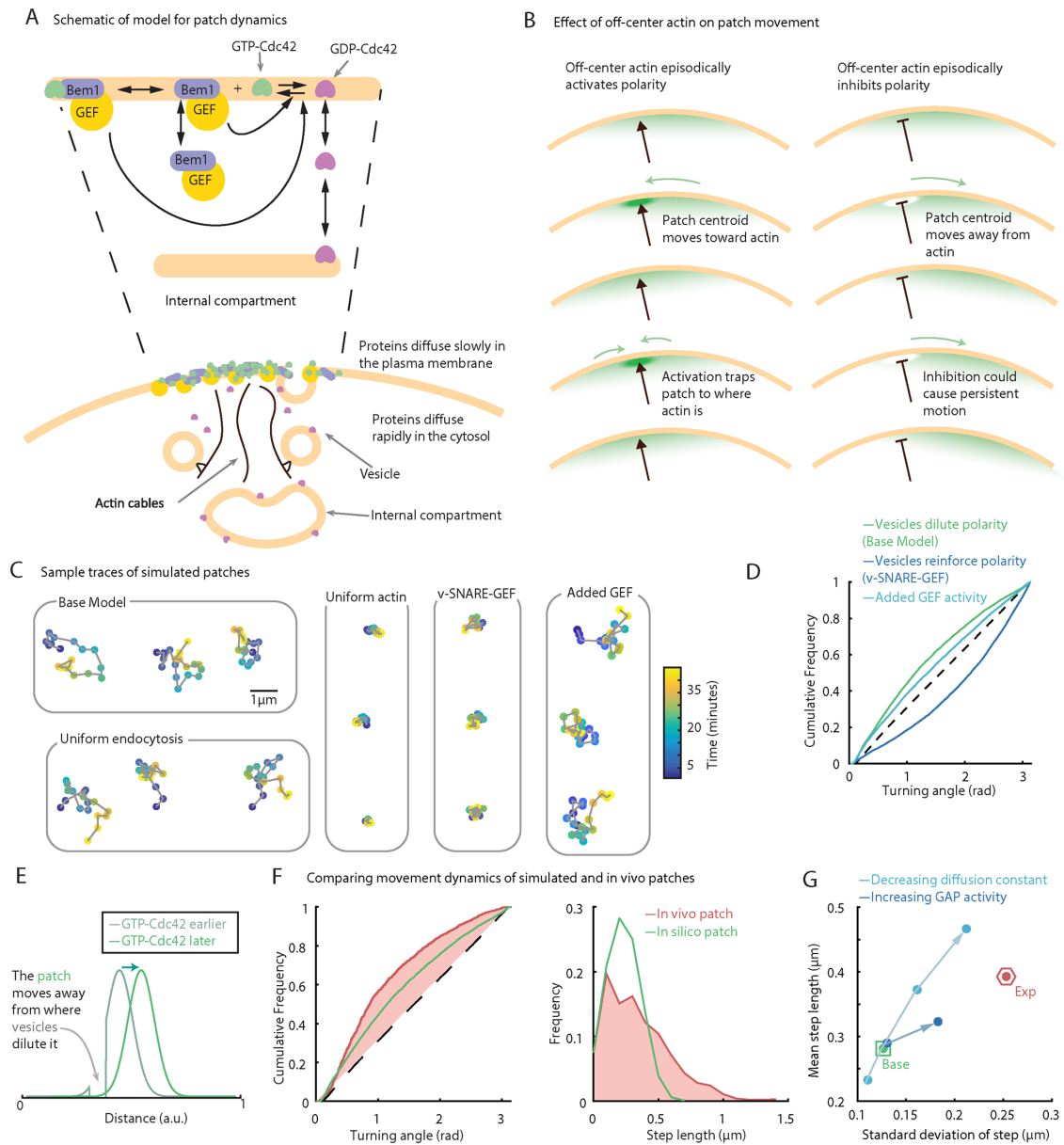


FIGURE 3: Mechanism of patch movement in computational model combining polarity factor dynamics and vesicle traffic. (A) Schematic of the model. Biochemical interactions coupled with protein diffusion (polarity module: top). Stochastic vesicle traffic transfers membrane and cargo between an internal compartment and the plasma membrane (vesicle trafficking module: bottom). (B) Expected effect of asymmetrically located actin depends on whether actin activates or inhibits polarity. Episodically activating polarity would trap the patch where the actin is (left), while inhibiting polarity would make the patch move persistently away from the actin (right). (C) Sample movement traces of simulated patch across four different conditions. Base model: focused exocytosis and endocytosis. Uniform actin: randomly located exocytosis and endocytosis. Uniform endocytosis: focused exocytosis with random endocytosis. v-SNARE-GEF: vesicles carry a species that reinforces polarity. Detailed histograms in Supplemental Figure S5. (D) Cumulative frequency plot of turning angles of the patch in the Base Model (where vesicles dilute polarity: green), Added GEF (where GEF activity is higher: light blue) and v-SNARE-GEF model (where vesicles reinforce polarity: blue). Dashed line is expected cumulative frequency if turning angles were sampled from a uniform distribution. The Base Model and added GEF exhibit persistence in the direction of motion, whereas the v-SNARE-GEF model exhibits anti-persistence. (E) Dilution by asymmetric vesicles shifts the patch centroid away from site of dilution. (F) Cumulative frequencies of turning angles and histogram of step lengths of simulated patch movement (green) compared with in vivo data (red and shading). (G) Mean vs. SD of step length distributions of the Base Model (green box) compared with models with decreasing membrane diffusion constant (light blue: $0.015 \mu\text{m}^2/\text{s}$, $0.0015 \mu\text{m}^2/\text{s}$, $0.0005 \mu\text{m}^2/\text{s}$) or increasing GAP activity (dark blue: $0.7/\text{s}$, $0.9/\text{s}$). Red hexagon: distribution from experimental measurements.

with increasing σ . For this set of step length distributions, the fraction of successful encounters between patches increased with the SD (Figure 2C).

Several of the largest steps in cells were caused by patches disappearing and reappearing in another part of the cell (Supplemental Figure S3, A–C). To understand the contribution of such events to

the search process, we ran simulations as before, but omitting step lengths larger than 1.5 μm . This led to a considerably lower search efficiency (Figure 2C). We conclude that a mixture of large and small steps enables patches to search for each other more effectively, consistent with findings from search processes for planar spaces (Humphries and Sims, 2014).

Modeling patch movement in silico

Computational modeling has provided significant insight into the behavior of complex systems, including the yeast polarity circuit (Johnson *et al.*, 2011; Chiou *et al.*, 2017; Goryachev and Leda, 2017). Minimalistic models encapsulate complex biochemistry and cell biology into simple black-box processes: these have been used to argue that negative feedback with a time delay (Ozbudak *et al.*, 2005) or molecular noise (Lawson *et al.*, 2013; Hegemann *et al.*, 2015) could in principle yield patch movement. A more complex, mechanistic model has also shown that vesicle traffic can yield movement of the polarity patch (Dyer *et al.*, 2013; McClure *et al.*, 2015). In this section, we first summarize the cell biological findings that motivated the mechanistic model and then discuss how the modeling framework encapsulates those findings.

Cell biology underpinning the yeast polarity model. Cell polarity in yeast is regulated by the Rho-family GTPase Cdc42, a protein that switches between active (GTP-Cdc42) and inactive (GDP-Cdc42) forms. Active Cdc42 at the plasma membrane provides positive feedback by recruiting a protein complex from the cytoplasm containing a Cdc42 effector, p21-activated kinase (PAK: omitted from the figure for simplicity), the scaffold protein Bem1, and the guanine nucleotide exchange factor (GEF), Cdc24 (Kozubowski *et al.*, 2008) (Figure 3A). The GEF activates neighboring inactive Cdc42, triggering a local chain reaction where newly activated Cdc42 activates nearby Cdc42, generating a polarity patch with a high local concentration of GTP-Cdc42. Once the patch has formed, the component polarity proteins dynamically exchange between the patch and the cytoplasm on a timescale of 2–4 s (Wedlich-Soldner *et al.*, 2004; Slaughter *et al.*, 2011; Dyer *et al.*, 2013). The longevity of the patch in the face of constant self-renewal suggests that it exists in a steady state in which activation of Cdc42 and recruitment of GEF is balanced by Cdc42 inactivation and GEF unbinding (Johnson *et al.*, 2011; Chiou *et al.*, 2018).

Cdc42 is prenylated and tethered to the inner leaflet of the plasma membrane, and the spread of GTP-Cdc42 is constrained by slow diffusion at the membrane (Valdez-Taubas and Pelham, 2003; Bendezú *et al.*, 2015; Sartorel *et al.*, 2018). However, the mobility of GDP-Cdc42 is considerably greater, both at the membrane (Bendezú *et al.*, 2015; Sartorel *et al.*, 2018) and because it can detach from the membrane to the cytosol, where diffusion is much more rapid. GDP-Cdc42 exchange between the plasma membrane and cytosol is mediated mainly by a guanine nucleotide dissociation inhibitor (GDI) (Johnson *et al.*, 2009). The GDI masks Cdc42's prenyl group and this rapidly reversible binding allows the GDI to pluck GDP-Cdc42 from one location on the plasma membrane, diffuse rapidly in the cytoplasm, and deposit the GDP-Cdc42 at another location (Garcia-Mata *et al.*, 2011; Johnson *et al.*, 2011; Woods *et al.*, 2016). When high-mobility GDP-Cdc42 is deposited at the polarity patch, it can become activated by the locally enriched GEF, trapping it at the membrane and further concentrating the local GTP-Cdc42. The "capture" of cytoplasmic proteins (GDP-Cdc42 and GEF) by membrane proteins in the polarity patch depletes cytoplasmic pools, which restricts the size of the polarity patch (Woods and Lew, 2019).

At the polarity patch, GTP-Cdc42 binds effectors called formins that nucleate polymerization of actin to make actin cables (Goode and Eck, 2007). The actin barbed ends are oriented toward the patch, allowing myosin V motors to deliver secretory vesicles to the patch, where they fuse with the plasma membrane by exocytosis (Figure 3A, bottom). These vesicles carry cell wall remodeling components that mediate focused growth and cell–cell fusion (not shown). They also add membrane area to the site of fusion, diluting resident factors.

Secretory vesicles originate at internal membranes (including trans-Golgi and endosomes), and endocytic vesicles travel back from the plasma membrane to the internal membranes. Imaging of secretory vesicle and endocytosis markers showed that exocytosis is tightly focused toward the polarity patch, while endocytic events occur over a broader area surrounding a wandering patch (McClure *et al.*, 2015). Most polarity factors, including Bem1 and the GEF Cdc24, are thought to associate with the plasma membrane by binding from the cytoplasm. This is also true for Cdc42, but in addition some Cdc42 is present on internal membranes and secretory vesicles, albeit at a lower concentration than at the polarity patch (Richman *et al.*, 2002; Watson *et al.*, 2014).

As mentioned in the *Introduction*, polarity patch movement is dependent on F-actin, suggesting that factors able to influence the polarity patch may be delivered or removed from the plasma membrane near the patch in an actin-dependent manner. Symmetry considerations dictate that if such delivery/retrieval were accurately centered on the centroid of the polarity patch, it would not cause any net displacement. However, a stochastic asymmetry in actin distribution with respect to the polarity patch could cause patch movement. Figure 3B illustrates two conceptual mechanisms by which this could occur. We begin by assuming that at some initial time the actin localizes predominantly on one side (here, arbitrarily, the left) of the polarity patch centroid. If actin strengthened polarity on that side, then the polarity patch centroid would shift leftward (Figure 3B, left column), whereas if actin weakened polarity on that side, then the polarity patch centroid would shift rightward (Figure 3B, right column). In the strengthening scenario, the patch would stop moving once the actin and the centroid were aligned. If the patch moved beyond the actin, it would switch directions and return (Figure 3B, left column). But in the weakening scenario, the patch centroid would keep moving away from the actin (Figure 3B, right column). These considerations suggest that to obtain persistent motion such as that observed in cells, actin should somehow weaken polarity. This is consistent with the general class of models in which negative feedback can lead to wavelike motion: as actin is itself localized in response to the polarity factors, a polarity-weakening effect of actin would constitute a negative feedback loop.

The mechanistic computational model discussed below combines a simplified biochemistry of the polarity circuit (the "polarity module") with a model for vesicle trafficking (including both exocytosis and endocytosis: the "vesicle trafficking module"). It tracks concentrations of various proteins on a discretized 2D surface with periodic boundary conditions representing the plasma membrane. There are also cytoplasmic and internal membrane compartments; because of their much higher diffusion, these compartments are considered well mixed. As polarity dynamics occur on rapid timescales relative to cell growth or Cdc42 synthesis/degradation, we also assume that the system has constant volume, membrane area, and protein content.

Mathematical model: polarity module. Cdc42 behavior is modeled as a system of PDEs encoding the biochemical reactions illustrated in Figure 3A and listed in Table 1, adapted from an original

Biochemical reactions			
Reaction	Rate constant	Value	Reference
$BemGEF_c \rightarrow BemGEF$	k_{1a}	10 s^{-1}	(Goryachev and Pokhilko, 2008; Savage et al., 2012)
$BemGEF \rightarrow BemGEF_c$	k_{1b}	10 s^{-1}	(Goryachev and Pokhilko, 2008; Savage et al., 2012)
$BemGEF + Cdc42D \rightarrow Cdc42T$	k_{2a}	$0.16 \mu\text{M}^{-1} \text{ s}^{-1}$	(Savage et al., 2012)
$Cdc42T \rightarrow Cdc42D$	k_{2b}	0.63 s^{-1}	(Savage et al., 2012)
$BemGEF42 + Cdc42D \rightarrow Cdc42T$	k_3	$0.35 \mu\text{M}^{-1} \text{ s}^{-1}$	(Savage et al., 2012)
$BemGEF + Cdc42T \rightarrow BemGEF42$	k_{4a}	$10 \mu\text{M}^{-1} \text{ s}^{-1}$	(Goryachev and Pokhilko, 2008; Savage et al., 2012)
$BemGEF42 \rightarrow BemGEF + Cdc42$	k_{4b}	10 s^{-1}	(Savage et al., 2012)
$Cdc42 \rightarrow Cdc42_c$	k_{5a}	144 s^{-1}	(Dyer et al., 2013)
$Cdc42_c \rightarrow Cdc42$	k_{5b}	20.8 s^{-1}	(Dyer et al., 2013)
$BemGEF_c + Cdc42T \rightarrow BemGEF42$	k_7	$10 \mu\text{M}^{-1} \text{ s}^{-1}$	(Dyer et al., 2013)

Model specifications			
Parameter	Value	Comments	Reference
Cell radius	$2.5 \mu\text{m}$		(Savage et al., 2012)
Membrane to cytoplasm volume ratio (η)	0.01		(Savage et al., 2012)
Membrane diffusion constant	$0.0045 \mu\text{m}^2 \text{ s}^{-1}$		(Dyer et al., 2013)
Cytoplasmic diffusion constant	Assumed well-mixed		(Savage et al., 2012)
Internal membrane diffusion constant	Assumed well-mixed		(Savage et al., 2012)
Mean [Cdc42] in cell	$1 \mu\text{M}$	39415 molecules in $65.4 \mu\text{m}^3$	(Goryachev and Pokhilko, 2008; Savage et al., 2012)
Mean [BemGEF] in cell	$0.017 \mu\text{M}$	670 molecules in $65.4 \mu\text{m}^3$	(Goryachev and Pokhilko, 2008; Savage et al., 2012)

TABLE 1: Biochemical reactions and parameter values for the polarity module.

model by Goryachev and Pokhilko (Goryachev and Pokhilko, 2008). Proteins in the model can reside on the plasma membrane, or the cytoplasm (indicated by the suffix c), or an internal membrane compartment (indicated by the suffix ic). A single “BemGEF” species is used to represent the components of the PAK/Bem1/GEF complex. BemGEF exchanges between plasma membrane and cytoplasm, undergoes reversible binding to GTP-Cdc42 at the membrane, and while at the membrane, it catalyzes exchange of GDP-Cdc42 to GTP-Cdc42 with mass action kinetics (Table 1).

The reactions catalyzed by Cdc42-directed GAPs and the GDI are present in the model, even though explicit GAP and GDI species are not. A first-order GTP hydrolysis reaction is used to represent the effects of GAP activity, and association/dissociation of GDP-Cdc42 with membranes is used to represent the effects of GDI (and potentially other chaperones; Woods et al., 2016). GDP-Cdc42 can associate with both the plasma membrane and the internal membrane compartment, whereas BemGEF (and hence GTP-Cdc42) only associates with the plasma membrane.

Mathematical model: vesicle trafficking module. Vesicle trafficking is modeled as a series of exocytosis and endocytosis events, with parameters listed in Table 2. Exocytosis is modeled as the instantaneous transfer of membrane area from the internal compartment to the plasma membrane, and endocytosis is modeled as a

transfer in the opposite direction. Individual exocytic or endocytic events occur as Poisson processes. The probabilities (and thus, rates) of exocytosis and endocytosis events per unit time are matched so that (except for minor fluctuations) there is no net transfer of membrane from one compartment to another. The area of an exocytic vesicle is about four times larger than that of an endocytic vesicle, and the plasma membrane is discretized into a 100×100 grid, where each grid element has approximately the same area as a single endocytic vesicle; thus, the total plasma membrane area is set to equal to that of 10,000 endocytic vesicles, or 2500 exocytic vesicles (Table 2).

To exploit the extensive experimental data on trafficking of integral membrane proteins in yeast, we include another molecular species, called v-SNARE, that controls the distribution and timing of endocytic events. This endocytic cargo species has properties that match the well-studied behavior of the yeast v-SNAREs Snc1 and Snc2 (Valdez-Taubas and Pelham, 2003). v-SNARE is present on both the internal membrane and the plasma membrane and is trafficked between them via exo- and endocytosis. It does not react biochemically with any polarity protein.

Exocytosis inserts a new vesicle-sized patch of membrane into the much larger plasma membrane, affecting the local concentrations of membrane-associated proteins. At the insertion site, new concentrations are set to equal those on the vesicle. Elsewhere on

Parameter	Value	Reference
Endocytosis rate	200 vesicles/min	(Dyer <i>et al.</i> , 2013)
Exocytosis rate	50 vesicles/min	(Dyer <i>et al.</i> , 2013)
Size of endocytic vesicle	0.00785 μm^2	(Prescianotto-Baschong and Riezman, 1998; Layton <i>et al.</i> , 2011)
Size of exocytic vesicle	0.0314 μm^2	(Novick <i>et al.</i> , 1980; Layton <i>et al.</i> , 2011)
Membrane diffusion constant for vSNARE	0.0025 $\mu\text{m}^2\text{s}^{-1}$	(Valdez-Taubas and Pelham, 2003; Dyer <i>et al.</i> , 2013)

TABLE 2: Parameters for vesicle trafficking module.

the plasma membrane, concentrations are calculated from the pre-existing concentration profiles of each species before vesicle fusion, according to a radial interpolation scheme (see Supplementary Figure S2 in Savage *et al.*, 2012 for details). This preserves a discretized grid with the same number of elements, and the size of each element is adjusted slightly to account for the increase in plasma membrane area due to vesicle fusion. After fusion, the membrane of the inserted vesicle is diffusionally connected to the rest of the plasma membrane, and concentrations evolve according to the reactions listed above.

Endocytosis is modeled in two steps to reflect the cell biology of the process. In the first step, the site of endocytosis becomes a diffusion sink for v-SNARE. This reflects the biological formation of a “coat” of proteins including clathrin and adaptor proteins that provide a high density of binding sites that trap endocytic cargo molecules. Accumulation of a preset threshold of v-SNARE triggers the second step, where the vesicle membrane is removed from the plasma membrane and added to the internal membrane (Layton *et al.*, 2011). The proteins that were associated with the membrane that endocytoses are redistributed as follows: v-SNARE and Cdc42 are added to the internal compartment, while BemGEF is returned to the cytoplasm. The concentrations of plasma membrane proteins following endocytosis are calculated from preexisting concentration profiles of each species according to a radial interpolation scheme, and the size of each discretization element is adjusted slightly to account for the decrease in plasma membrane area due to vesicle fission.

Connecting the polarity and vesicle trafficking modules. Vesicle traffic affects polarity factor concentration profiles by inserting or removing membrane and cargo at specific locations. In turn, polarity factors affect membrane traffic by influencing the location of exocytic and endocytic events. Here we discuss how the spatial location of exocytic and endocytic events is determined in the model.

In cells, GTP-Cdc42 is thought to promote local exocytosis by orienting actin cables toward the polarity site (Evangelista *et al.*, 1997) and promoting fusion of vesicles that reach that site (Adamo *et al.*, 2001). There are approximately 10 actin cables oriented toward the polarity patch (Yu *et al.*, 2011), and in the model we allow exocytosis to occur at one of only 10 sites, representing actin cable termini. We assume that new actin cables form in a manner influenced by the local GTP-Cdc42 concentration and set the probability of actin cable attachment at a given location as a Hill function of the GTP-Cdc42 concentration at that location:

$$P_{\text{cable}}(x, y) = \frac{1}{Z} \frac{[\text{Cdc42T}(x, y)]^4}{k_{\text{Cdc42T}}^4 + [\text{Cdc42T}(x, y)]^4}$$

Here, $P_{\text{cable}}(x, y)$ is the probability of attaching a cable at location (x, y) , $\text{Cdc42T}(x, y)$ is the GTP-Cdc42 concentration at (x, y) , k_{Cdc42T} is set to 50% of the maximum GTP-Cdc42 concentration, and Z is a

normalization factor. Once formed, cables are assumed to remain stationary until they detach or depolymerize. Detachment occurs on a 1-min timescale (rate 1 min^{-1}) and allows attachment of a new cable. The model generally has 10 sites demarcated as potential exocytosis sites at any given time, and we assume that each of those is equally likely to serve as the site for exocytosis.

The mechanism that determines the spatial pattern of endocytic events in cells is not understood. However, endocytic cargo proteins probably play a role: because they are delivered by exocytosis, their concentration (like that of v-SNARE in the model) would be higher near the polarity site where endocytic events cluster. We model the probability that an endocytic event takes place at a given location as a Hill function of the v-SNARE concentration at that location.

$$P_{\text{endo}}(x, y) = \frac{1}{Z} \frac{[\text{vSNARE}(x, y)]^4}{k_{\text{vSNARE}}^4 + [\text{vSNARE}(x, y)]^4}$$

Here, $P_{\text{endo}}(x, y)$ is the probability of attaching a cable at location (x, y) , $\text{vSNARE}(x, y)$ is the v-SNARE concentration at (x, y) , k_{vSNARE} is set to 50% of the maximum v-SNARE concentration, and Z is a normalization factor. This yields a spatial distribution of endocytic events in the model similar to that observed in cells (McClure *et al.*, 2015).

Mechanism of patch movement in the model. Simulation of the model discussed above (henceforth, the “Base Model”), where exocytosis and endocytosis events are coupled to the polarity circuit, leads to the formation of a polarity patch enriched for GTP-Cdc42, whose centroid wanders around the plasma membrane. Sample traces of patch movement in the Base Model are shown in Figure 3C. The polarity module alone produces a stable, stationary polarity patch (Goryachev and Pokhilko, 2008), demonstrating that stochastic vesicle traffic drives polarity patch movement. However, it is not intuitively obvious what aspect of vesicle trafficking (exocytosis or endocytosis) causes the patch to move. To assess the relative contributions of focused exocytosis and endocytosis, we modified the model in two ways.

First, we allowed the 10 actin cables to attach with uniform probability all over the plasma membrane. In these simulations, exocytosis events occur at random sites that are often distant from the patch. Because v-SNARE delivery is no longer polarized, endocytic events also occur in a distributed manner. Although similar numbers of vesicles are trafficked to and from the plasma membrane in these simulations, traffic was no longer focused on the polarity site, and the polarity site stopped moving (Figure 3C, Uniform exocytosis). Thus, focused vesicle trafficking is essential for patch movement.

Second, we retained focused actin cables and hence focused exocytosis, but made the spatial location of endocytic events random. In these simulations, polarity patch movement was comparable to that in the full model (Figure 3C, Uniform endocytosis), indicating that it is focused exocytosis, rather than focused endocytosis, which drives patch movement.

Previous studies had proposed that secretory vesicles could strengthen polarity by delivering Cdc42 (Wedlich-Soldner *et al.*, 2003), or weaken polarity by diluting Cdc42 and other polarity factors (Layton *et al.*, 2011; Savage *et al.*, 2012). A yeast strain was engineered to concentrate polarity factors on secretory vesicles by fusing Bem1 to a v-SNARE, which is highly enriched on secretory vesicles. This led to dramatically reduced patch movement in mating cells (Dyer *et al.*, 2013). Similarly, a model in which the v-SNARE was endowed with GEF activity caused the *in silico* patch to stall (Figure 3C, v-SNARE-GEF). We confirmed that the stalling in the v-SNARE-GEF model was not simply because of higher overall GEF activity (due to the presence of both v-SNARE-GEF and native GEF) on the membrane: Increasing BemGEF activity (k_3) in the Base Model to match the amount of added v-SNARE-GEF did not stall the patch (Figure 3C, Added GEF), confirming that the patch stalling in the v-SNARE-GEF model was not simply due to higher overall GEF activity. Sample simulations of the patch moving due to vesicle dilution and the patch being stalled by v-SNARE-GEF are shown in Supplemental Movies S1 and S2, respectively.

To better understand how concentrating polarity factors on secretory vesicles stalled patch movement, we extracted turning angle distributions from traces of patch centroids in model simulations. In the Base Model, there was a preference for small turning angles, indicating that patch movement is persistent, as it is *in vivo*. This remained true with additional BemGEF activity (“Added GEF” in Figure 3D), but in the model with v-SNARE-GEF, patch movement was anti-persistent: that is, rather than being more likely to keep moving in the same direction, the patch tended to reverse direction (Figure 3D). This is consistent with the proposal (above) that if actin (in this case cable-mediated exocytosis) were to strengthen polarity, that would tend to reverse any excursions of the patch away from the actin. These simulations confirm that actin must weaken polarity in order to drive persistent patch movement.

The simplest mechanism by which exocytic events could weaken the polarity patch is by local dilution of polarity factors (Dyer *et al.*, 2013; McClure *et al.*, 2015). When an exocytic vesicle fuses within (but not at the center of) the polarity patch, it transiently dilutes polarity factors on the side of the patch where it fuses. For a brief time following fusion, recruitment of new polarity factors from the cytoplasm occurs more efficiently on the opposite (undiluted) side of the patch, causing the patch centroid to move away from the vesicle fusion site (Figure 3E). This transient effect of each vesicle is not reversed by endocytosis, which seems to contribute little to patch movement. Thus, in the model, patch movement arises due to repeated exocytic vesicle fusion events near the patch, which affect the location of the patch centroid by diluting polarity factors at the site of fusion.

Comparison of patch movement in silico and in vivo

To compare patch movement in the model with that in cells, we extracted step length and turning angle distributions from traces of patch centroids in model simulations sampled at 1.5-min intervals (Figure 3F). Polarity patches in the Base Model exhibited smaller and less variable step sizes (Figure 3F, left). We focused on step lengths below 1.5 μm because the rare larger steps observed experimentally were a result of the patch disappearing and reappearing at another part of the cell (disappearing patches are seen in < 2% of time points; see Supplemental Movie S3), which was a behavior not recreated by the Base Model (see *Discussion*). Moreover, the distribution of turning angles was more uniformly distributed than those taken by patches in cells, indicating that movement is less persistent in the Base Model (Figure 3F, right).

In principle, the differences between the patch movement *in vivo* and *in silico* could indicate that the movement mechanisms encoded in the model are insufficient to explain the degree of patch movement. Alternatively, it could be that tweaking model parameters would produce movement comparable to that in cells.

Since vesicles drive patch movement by diluting polarity factors, patch movement could presumably be increased by increasing either the area of individual exocytic vesicles or the frequency of exocytosis. However, these parameters (or, more precisely, the average values of these parameters) are tightly constrained by experimental data, so this does not seem like a plausible explanation for the discrepancy between model and experiment. On the other hand, the biochemical parameters of the polarity module are less constrained, and previous work suggested that increasing GAP activity (which lowers GTP-Cdc42 concentration in the patch) or decreasing membrane diffusion (to make the patch smaller) might make the polarity patch more susceptible to perturbation by vesicles (Dyer *et al.*, 2013). Increasing GAP activity did increase mean step length slightly, but raising the GAP activity further made the polarity patch collapse before the mean step length could match that observed in cells (Figure 3G). Lowering Cdc42 diffusion also increased mean step length, but the diffusion constants required to match the step lengths in cells were far below experimentally the estimated diffusion constants (Marco *et al.*, 2007; Sartorel *et al.*, 2018) (Figure 3G). Thus, tweaking model parameters failed to match experimental data within plausible ranges. We wondered whether features of vesicle traffic not yet included in the model might account for the discrepancy between *in vivo* and *in silico* patch movement.

Biologically inspired model adjustments can align in silico and in vivo patch movement

In the Base Model, the spatial distribution of actin cables, and hence of exocytic vesicle fusion sites, is determined by the distribution of GTP-Cdc42. As a consequence, polarity protein and actin/vesicle distributions are very similar (Figure 4A). However, in cells, it has been noted that the formin-binding protein Spa2 (Lawson *et al.*, 2013) and the exocytic vesicle marker Sec4 (McClure *et al.*, 2015) exhibit more tightly focused distributions. We imaged Spa2, the formin Bni1, the secretory vesicle Rab GTPase Sec4, and the exocyst component Exo70 (the exocyst is a complex that tethers secretory vesicles to the plasma membrane and promotes their fusion) in our cells with moving patches. In all cases, these actin cable/secretory vesicle markers were tightly colocalized (Figure 4, B–D) and displayed a considerably more focused distribution than that of the polarity markers Cdc42, Cdc24, and Bem1 in the same cells (Figure 4, E–G). Thus, cells can cluster actin cable termini, and the vesicles transported by cables, to a narrower zone than that occupied by polarity factors.

To ask whether addition of a pathway to spatially cluster actin/vesicles in the model might alter patch movement, we took a phenomenological approach. Recall that the locations of actin cable formation in the Base Model are probabilistically determined by the spatial distribution of active Cdc42:

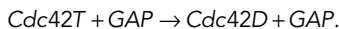
$$P_{\text{cable}}(x, y) = \frac{1}{Z} \frac{[\text{Cdc42T}(x, y)]^4}{k_{\text{Cdc42T}}^4 + [\text{Cdc42T}(x, y)]^4}$$

We altered the above equation so that the centroid of existing actin cables $[x_{\text{cen}}, y_{\text{cen}}]$ would also bias where actin cables form:

$$P_{\text{cable}}(x, y) = \frac{1}{Z} \frac{[\text{Cdc42T}(x, y)]^4}{k_{\text{Cdc42T}}^4 + [\text{Cdc42T}(x, y)]^4} \left(1 + k_{\text{GE}} \frac{(x-x_{\text{cen}})^2 + (y-y_{\text{cen}})^2}{2 \times \sigma^2} \right)$$

This introduces a Gaussian centered on the centroid of the pre-existing actin cable distribution, which affects the probability of local cable formation. The width of the Gaussian ($\sigma_a = 0.24 \mu\text{m}$) was estimated from Spa2-mCherry fluorescent intensity along the periphery of artificially arrested cells (see *Materials and Methods* and Supplemental Figure S4). Making new cables more likely to form in the vicinity of previously existing actin cables caused vesicle fusion to become more focused (Figure 5A), in a manner dependent on the parameter k_G . Increasing k_G narrowed the zone of vesicle delivery (Figure 5B) and caused the mean step length and persistence of patch movement to increase (Figure 5C; compare Supplemental Movie S1 with Supplemental Movie S4). However, the value of $k_G = 1$ (which allowed the model to match the experimental persistence) did not greatly increase the mean step length, while the value of $k_G = 5$ (which allowed the model to match the experimental mean step length) caused excessive persistence (Figure 5D). Thus, focusing vesicle delivery is a promising adjustment that improves model behavior, but it is not sufficient to recreate *in vivo* patch movement.

The displacement of the patch in the model is due to dilution of polarity factors on vesicle fusion, but we reasoned that the ability of exocytic vesicles to weaken polarity would be enhanced if vesicles also carried Cdc42 inhibitors. Indeed, it was suggested that delivery of Cdc42-directed GAPs on secretory vesicles promoted patch mobility in a different context (Ozbudak *et al.*, 2005), and the GAP Bem3 was detected on vesicles, at least when overexpressed (Knaus *et al.*, 2007; Mukherjee *et al.*, 2013). Thus, we tested the effect of incorporating a vesicle-delivered GAP species into our Base Model (Figure 5E). We assumed that following delivery to the plasma membrane, the GAP diffuses at the same rate as Cdc42 and detaches/decays with first-order kinetics. A new reaction was introduced to the model to account for the effects of the new GAP:



We explored the effect of varying GAP level on the vesicle and GAP detachment rate from the plasma membrane. Decreasing the GAP decay rate or increasing the GAP amount did not change persistence much (Figure 5F, left), but made the patch take larger steps (Figure 5F, right), consistent with the expectation that vesicles delivering GAPs would be more perturbing than vesicles without GAPs. While the patch also took slightly more variable steps, the vesicular GAP needed to obtain realistic mean step size did not increase the variability enough to match experimental step length distributions (Figure 5G). Interestingly, in simulations with vesicular GAPs the patch would sometimes split in two (Figure 5H) or get destroyed by vesicle traffic, which was not observed with the Base Model. Thus, vesicular GAPs could potentially explain the rare instances of such behavior observed in cells (Figure 5I).

While both focused actin cables and vesicle-associated GAPs made the patch move larger distances and more persistently, neither feature reproduced the large SD of step lengths observed experimentally. As discussed above, a mix of large and small steps is important to optimize the search process by which patches might locate partners, so we wondered how cells might achieve this high variability.

Increasing the rate of vesicle delivery made step lengths both larger and more variable (Figure 6A). Although the average rate of vesicle delivery is physiologically constrained, we considered the possibility that the rate of vesicle fusion events might fluctuate, with bursts of rapid fusion interspersed with periods of less frequent fusion. We reasoned that the periods of less frequent exocytosis would yield smaller steps while bursts of more frequent exocytosis would yield larger steps, creating a broader distribution of step lengths.

To investigate this hypothesis, we allowed the Base Model to switch between regimes with higher or lower rates of exocytosis and endocytosis (Figure 6B). Rates were matched to preserve the same relationship between exocytic and endocytic events, and switching probabilities between higher and lower rate regimes were set so that over time, the average rates of vesicle traffic would remain the same as in the original model (50 vesicle fusion events/min). In this scheme, the “burstiness” of vesicle traffic could be increased by varying the fusion rates in each regime (Figure 6, C and D); increasingly, heterogeneous vesicle traffic led to patch movement with step length distributions that were as variable as experimentally determined step length distributions, but with a much lower mean (Figure 6E).

In summary, the characteristics of polarity patch movement in cells differed from those in our Base Model in three ways, with the model showing less persistent movement, taking smaller steps on average, and taking less variable-sized steps. However, allowing vesicle fusion events to be more clustered in space produced more persistent movement in the model (Figure 5, B–D), allowing vesicle-mediated delivery of GAPs produced larger step sizes in the model (Figure 5, E–G), and allowing more irregular vesicle-fusion rates produced more variable step sizes in the model (Figure 6, C and D). While each of these features could not individually recapitulate *in vivo* patch movement, we reasoned that some combination may be able to do so. A manually curated parameter search for a model with all three features allowed us to closely match movement observed in the model to that observed in cells (Figure 6, F and G; Supplemental Movie S5), suggesting that perturbation by actin-directed vesicle traffic is sufficient to account for the observed movement.

We then asked how the various versions of the model would perform in mating partner search simulations like those in Figure 2. Sampling step lengths and turning angles from different versions of the model, we found that each feature (focused vesicle delivery, vesicle-associated GAPs, and irregular vesicle fusion rate) improved model performance in partner search over that of the Base Model. Moreover, the improvements were additive, with the model that incorporated all three features providing the most efficient search (Figure 6H).

DISCUSSION

Mechanism of polarity patch movement

In this study, we characterized undirected polarity patch movement in budding yeast cells induced to undergo a mating response and used a computational model to show that vesicle traffic polarized toward the patch could suffice to drive such movement. Our simulations suggest that movement is driven primarily by the focused delivery of exocytic vesicles to the patch by actin cables, with little contribution from focused endocytosis. To cause persistent movement, exocytic vesicle fusion must locally weaken polarity, providing negative feedback: simulations with vesicles that locally strengthened polarity stabilized the patch position and stalled patch movement.

The polarity patch is created and sustained by a dynamic biochemical positive feedback loop whereby active polarity factors at the membrane recruit more polarity factors from the cytoplasm, counteracting the continuous loss of polarity factors by lateral diffusion and detachment to the cytoplasm (Chiou *et al.*, 2017). By locally weakening polarity, vesicles fusing on one side of the patch create an asymmetry such that the opposing side of the patch is better at recruiting cytoplasmic factors, so that the centroid of the cluster of proteins that constitute the patch is shifted away from the vesicle fusion site (Figure 3E).

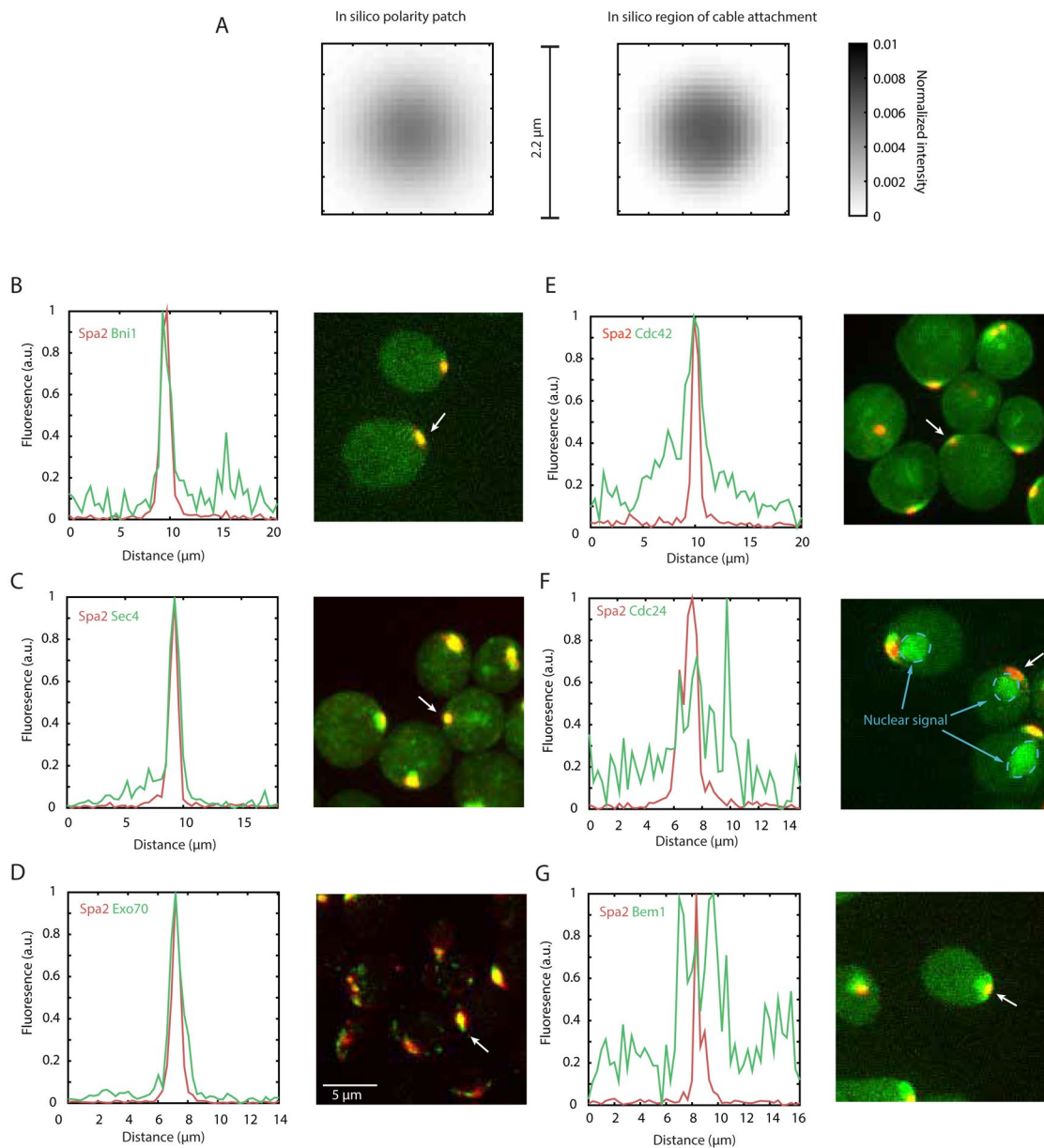


FIGURE 4: Vesicle delivery is focused to a greater degree than polarity proteins. (A) Normalized in silico polarity patch and region of actin cable attachment in the Base Model. (B–G) Left: normalized fluorescence intensity along the cell periphery of the indicated probes in cells induced to activate the mating pathway. Right: merged 2-color maximum projections of representative cells. White arrow: cell that was quantified. (B–D) The polarisome component Spa2 (red) colocalizes with the formin Bni1, which attaches actin cables (B: DLY23476), the Rab-family vesicle marker Sec4 (C: DLY23416), and the exocyst subunit Exo70, which tethers vesicles to the plasma membrane (D: DLY23451). (E–G) Spa2 distribution is more focused than that of polarity factors Cdc42 (E: DLY23421), the GEF Cdc24 (F: DLY21957, note that Cdc24 also localizes to the nucleus), and the scaffold Bem1 (G: DLY23418).

This mechanism spontaneously yields periods of persistent patch movement. Note that there would not be any net movement if vesicle fusion events were symmetrically distributed around the patch centroid. However, stochastic asymmetries in the distribution of actin cables within the patch occasionally lead to a shift of the polarity factor centroid away from the actin-enriched side. In turn, that leaves the actin cables further “behind” the polarity centroid, so that subsequent actin-delivered vesicles are more likely to shift the centroid in the same direction, creating persistent movement.

Our proposed mechanism of patch movement is fully consistent with experimental findings on the distribution of various proteins in

cells with moving polarity sites (Figure 7A). During periods of persistent movement, markers of vesicle fusion and actin termini colocalize, but they lag behind the polarity markers (McClure *et al.*, 2015). In turn, pheromone receptors and G proteins, which are delivered to the membrane on exocytic vesicles, accumulate behind the moving patch of vesicle markers (McClure *et al.*, 2015; Wang *et al.*, 2019).

How would vesicle fusion locally weaken polarity? We considered two mechanisms: dilution of polarity factors and delivery of polarity inhibitors. Fusion of a vesicle with the plasma membrane adds to the area of a polarity patch, thereby affecting local polarity factor concentrations. Because vesicles are thought to lack most

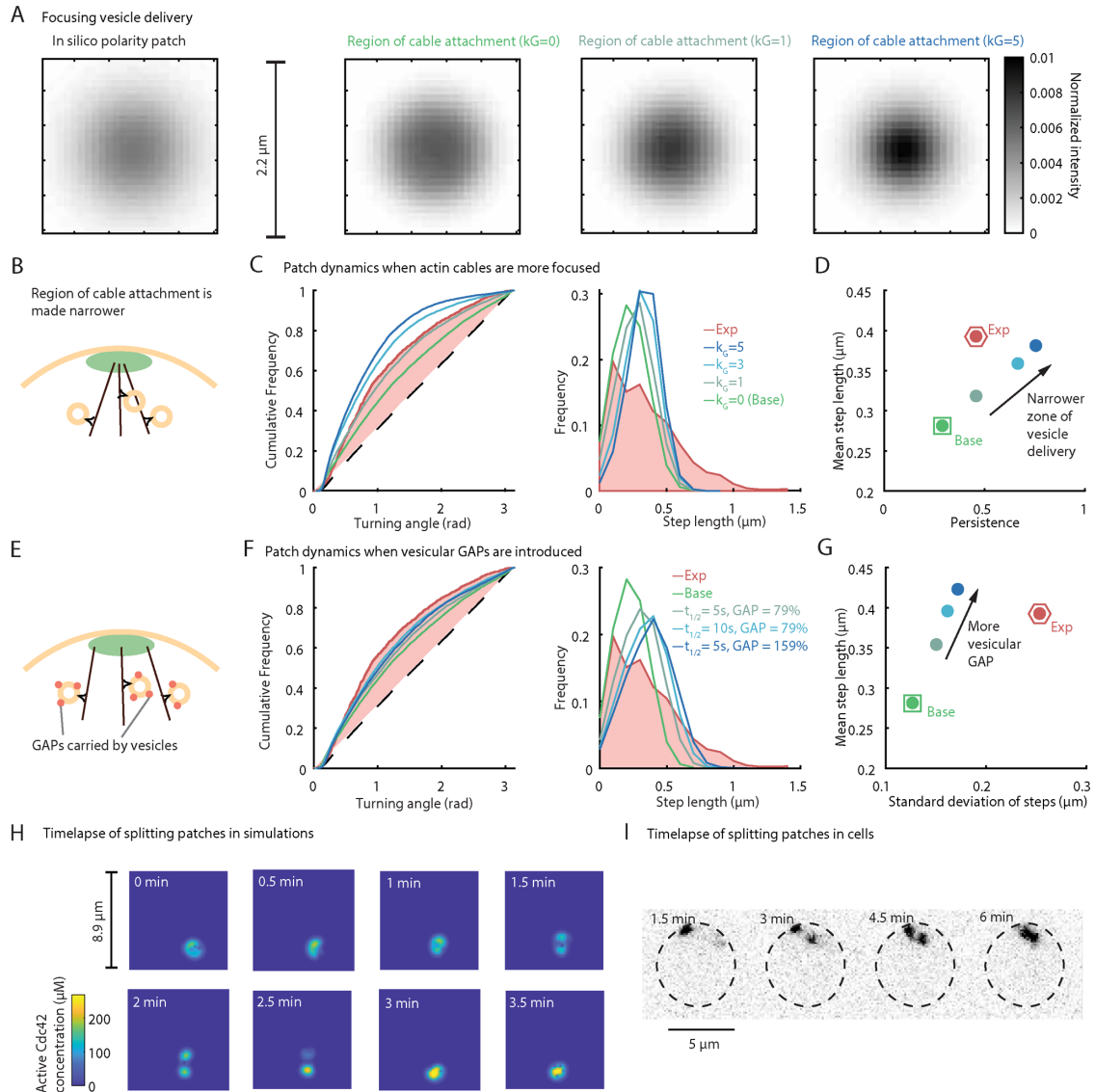


FIGURE 5: Effect of focusing vesicle delivery and incorporating vesicular GAPs on patch movement in silico. (A) Focusing of the region of actin cable attachment by increasing k_G in the model. (B) Cartoon: actin cables (black) are more focused than the polarity factors (green). (C) Cumulative frequency of turning angles (left) and histogram of step lengths (right) for models with increasing k_G . Red shading: experimental data. Green: Base Model. (D) Comparison of mean step length vs. persistence between the Base Model (green), experimental patch movement (red), and models with increasing k_G (colors matched to C). (E) Cartoon: vesicles carry GAPs (red dots) that inhibit Cdc42. (F) Cumulative frequency of turning angles (left) and histogram of step lengths (right) for models with different amounts of vesicular GAP and decay rates. Vesicular GAP indicated as X% of the basal GAP activity of 0.63 s^{-1} . Red shading: experimental data. Green: Base Model. (G) Mean vs. SD of step length distributions for the Base Model (green), experimental patch movement (red), and models increasing vesicular GAP (colors matched to F). (H) Time-lapse frames from simulation illustrate patch splitting behavior observed in the model with vesicular GAPs. (I) Inverted maximum projection snapshots from a cell that illustrates transient patch splitting. Cell with Spa2-GFP (DLY18172) induced to activate the mating pathway. Dashed line, cell outline.

polarity factors (Bem1, Cdc24, PAKs, etc.) and carry Cdc42 at a lower concentration than that present in the patch (Watson *et al.*, 2014), their main effect is to dilute polarity factors. One might argue that endocytosis should counteract this effect by removing membrane and thereby increasing polarity factor concentration. However, endocytic vesicles are smaller than exocytic vesicles: it takes four endocytic vesicles to retrieve the same area of membrane as that added by a single exocytic vesicle (Layton *et al.*, 2011; Dyer *et al.*, 2013). This means that membrane retrieval would likely be significantly less asymmetric than delivery, and the effects of asym-

metric membrane addition would not be counteracted by more symmetric membrane removal. Moreover, many endocytic events occur outside or at the periphery of the patch where they do not affect polarity factor concentrations. These considerations explain why in our simulations, the dilution effect from exocytic vesicles leads to patch movement that is insensitive to the location of endocytic events (Figure 3C).

In addition to polarity factor dilution, exocytic vesicles could deliver factors that inhibit polarity, such as Cdc42-directed GAPs. Experimental support for this hypothesis comes from the finding that

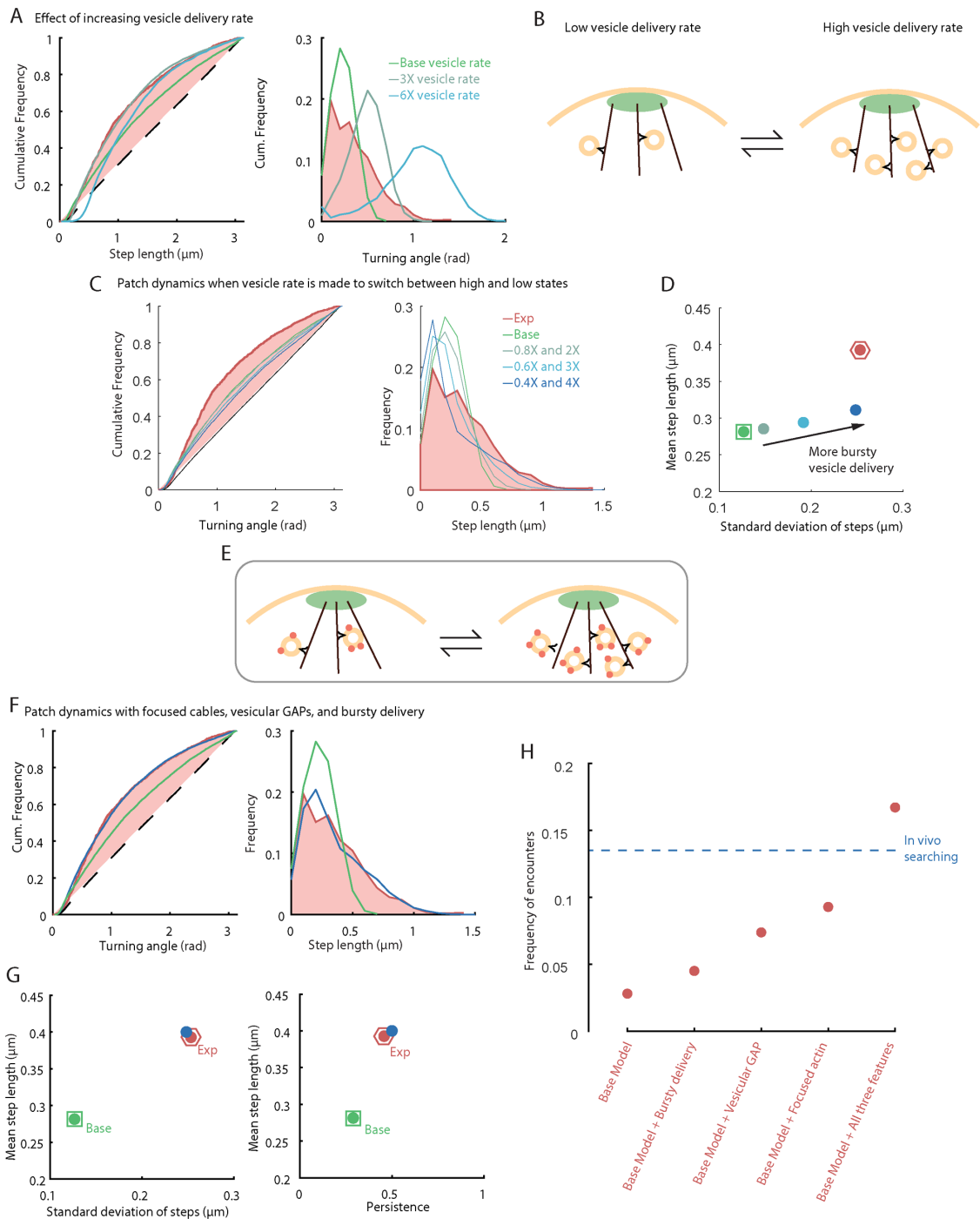


FIGURE 6: Effect of variable vesicle delivery rates on patch movement in silico, and quantitative matching of model and experiment. (A) Cumulative frequency of turning angles (left) and histogram of step lengths (right) for model with increasing vesicle delivery rates. (B) Cartoon: model switches between low and high vesicle delivery rates. (C) Cumulative frequency of turning angles (left) and histogram of step lengths (right) for models with variable vesicle delivery rates. Red shading: experimental data. Green: Base Model. We added temporally variable vesicle delivery to the Base Model and increased the difference between high and low states by varying vesicle rates such that the average delivery rate remained at physiological levels. The variable rates in the legend indicate the fold difference from the physiological rate. D Comparison of mean vs. SD of step lengths between the Base Model (green), experimental patch movement (red), and models with variable vesicle delivery rates (colors matched to C). (E) Cartoon: model that incorporates focused actin cables, vesicular Gaps, and variable rates of vesicle delivery. (F) Cumulative frequency of turning angles (left) and histogram of step lengths (right) for model in E. Red shading: experimental data. Green: Base Model. Blue: model in E. We used: focusing $k_G = 1.5$; vesicular GAP = 0.3 s^{-1} ; delivery rates = $0.5X$ and $0.3X$. (G) Comparison of mean vs. SD of step lengths (left) and mean step length vs persistence (right) between the Base Model (green), experimental patch movement (red), and the model in E (blue). H Search efficiencies for different models (red) and from in vivo data for steps less than $1.5 \mu\text{m}$ (dotted blue line).

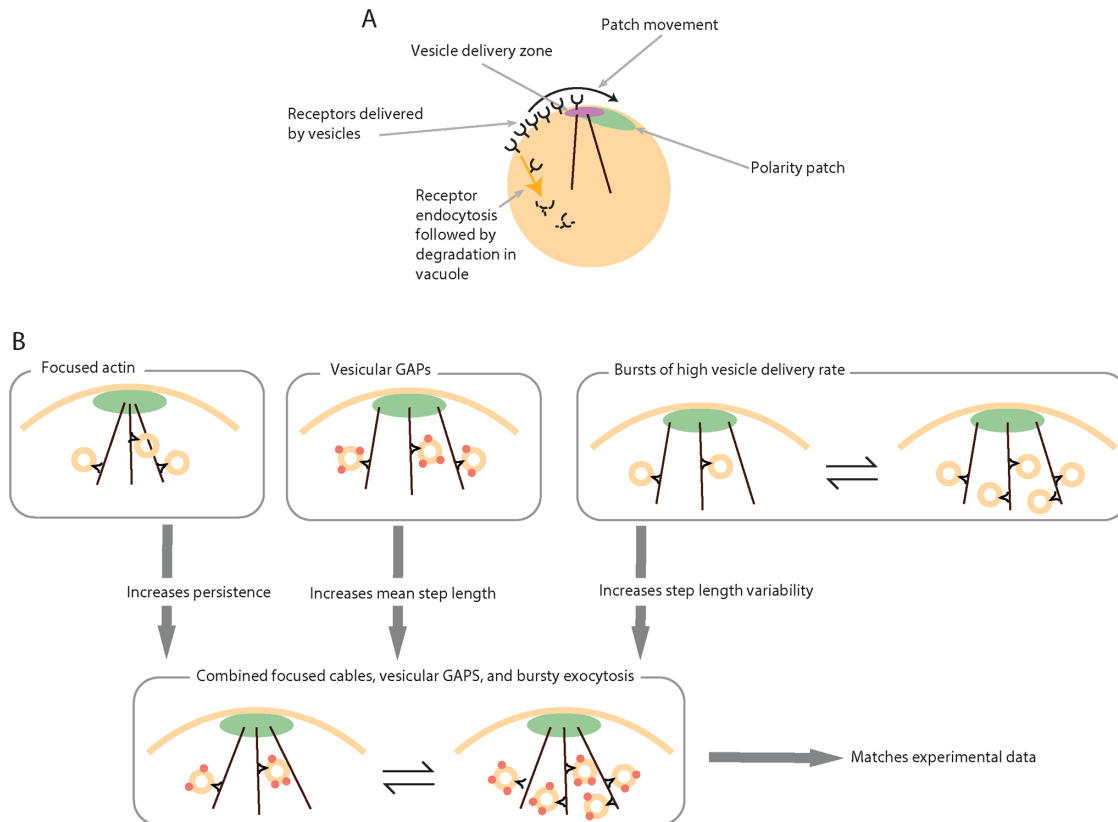


FIGURE 7: Focused vesicle delivery with yeast characteristics can account for polarity patch movement.

(A) Distributions of proteins during patch movement: In a persistently moving patch, polarity factors are followed by actin cables/exocytosis markers, which in turn lead the region where receptors are concentrated. (B) Adjustments to the computational model allows it to closely reproduce patch behavior in vivo.

the GAP Bem3 is enriched on secretory vesicles (Knaus *et al.*, 2007; Mukherjee *et al.*, 2013). A similar mechanism may apply in other systems, as the GAP REN1 is enriched on secretory vesicles in pollen tubes (Hwang *et al.*, 2008). The degree to which this may affect patch movement has yet to be experimentally tested in mating cells, but a quantitative effect of GAP deletions on the degree of patch movement has been noted in other contexts (Ozbudak *et al.*, 2005).

Focused vesicle traffic can produce movement quantitatively like that observed in cells

To compare the characteristics of patch movement in cells with those in the computational model, we measured the distributions of step sizes and turning angles from movies and simulations. This revealed that patch movement observed in our starting Base Model was less persistent (i.e., it had more random turning angles) than that observed in cells. In addition, patch movement in that model displayed smaller and more homogeneous step sizes than patch movement in cells. A feature that is notably absent in our model is the molecular noise that arises from diffusion and stochastic binding/unbinding events—omitted due to technical challenges associated with accurately simulating physiological noise. It is possible that the absence of molecular noise explains the quantitative discrepancies between patch movement in the Base Model and in cells. However, as the patch in cells moves very little when actin is depolymerized (Dyer *et al.*, 2013; Hegemann *et al.*, 2015; McClure *et al.*, 2015), molecular noise does not appear to be a potent mechanism for patch movement on its own, and it may not be the only relevant factor absent in the Base

Model. Instead, we considered three cell biological features that could bring the model simulations into better alignment with the data from cells.

First, cells display a distribution of actin cable termini and vesicle delivery/fusion markers that is more focused than that of polarity factors (Figure 4). Introduction of such focusing in the model created more persistent patch movement (Figure 5, B–D). Because movement is caused by stochastic vesicle fusion events that are off-center relative to the polarity patch, vesicles delivered to opposite sides of the patch reduce net patch movement. Narrowing the zone of vesicle delivery made it less likely for off-center vesicles to fuse on opposite sides of a patch, which made the patch travel further and more persistently. Second, allowing the rate of vesicle delivery to vary (while maintaining the same average delivery rate) led to a more variable distribution of the step sizes observed in model simulations (Figure 6, B–D). Third, introducing a GAP delivered by vesicles enhanced the degree to which each vesicle weakened the polarity patch. This led the patch to move further, increasing the average step size (Figure 5, E–G).

Another, unanticipated effect of vesicular GAPs was that the model sometimes displayed patches that transiently split in two (Figure 5H). This behavior was occasionally seen in our cells as well (Figure 5I). The split occurs due to accumulation of Cdc42 inhibitors (GAPs) within the patch, creating two spatially separated zones of active Cdc42 that compete with each other (Figure 5H). Such splitting fronts have been documented in *Dictyostelium* during locomotion (Neilson *et al.*, 2011; Shi *et al.*, 2013) and in *Ashbya* during branched hyphal growth (Ayad-Durieux *et al.*, 2000). Moreover, patches in cells displayed another infrequent behavior, disappearing

and then reappearing at another location on the cell cortex that was not seen in the model. However, addition of stronger vesicular GAPs in the model could destroy the patch completely, and if noise were present a new patch could form elsewhere. Thus, vesicle-associated GAPs could help to explain the rare events where patches are seen to split or relocate in cells.

Interestingly, studies of mating in the distantly related fission yeast identified a search process, dubbed “speed dating,” in which polarity patches formed and then disappeared at different sites on the cell cortex (Bendezú and Martin, 2013; Merlini *et al.*, 2016). As noted above, GAP delivery on vesicles could cause patch disappearance in our model, and a recent report indicated that deleting a GAP that is targeted to the polarity site in fission yeast led to movement of the polarity site, as observed in budding yeast (Castro and Martin, 2018). Thus, although patch appearance/disappearance (in fission yeast) and patch movement (in budding yeast) may seem like different behaviors, the underlying mechanism may be similar.

Together, a combination of spatially focused vesicle delivery, temporally varying vesicle delivery rates, and vesicular GAPs can recreate patch turning angle and step length distributions that closely match those observed in cells (Figure 7B). Thus, focused vesicle traffic could plausibly account for the patch movement in cells.

Our analysis of patch movement in the model was done by transferring results obtained from planar simulations onto a spherical surface. Studies of polarity models on different geometries have reported that patches may have an affinity for (Maree *et al.*, 2012; Vandin *et al.*, 2016) or aversion toward (Trogon *et al.*, 2018) regions of high curvature, depending on the specifics of each model. Thus, nonspherical cell geometry has the potential to bias patch dynamics.

Relevance beyond budding yeast

As discussed above, polarity patch movement in yeast arises from the coupling of a polarity circuit with strong positive feedback to a cell biological negative feedback enacted by actin cable-mediated vesicle delivery. This is one instantiation of a class of models discussed by Meinhardt in the context of axon guidance (Meinhardt, 1999). In such systems, the positive feedback generates a strong spatially focused signal that defines a cell’s front. Positive feedback comes at a cost, however, because by reinforcing the front such feedback makes its position insensitive to external cues. Local weakening of the front by a delayed local negative feedback allows relocation and makes the front more sensitive to external cues. As with yeast polarity proteins, the factors that define a cell’s front in other systems direct movement or growth up chemical gradients. Many of these systems involve interacting positive and negative feedback loops. Germinating spores of fission yeast display mobile Cdc42-enriched fronts thought to arise from positive feedback in the Cdc42 system coupled to negative feedback by mechanical stimuli from the cell wall (Bonazzi *et al.*, 2014). In frog oocytes and echinoderm embryos, Rho signaling is similarly coupled with actin-mediated feedback in an excitable system that generates traveling waves (Bement *et al.*, 2015). In *Dictyostelium* amoebae and mammalian neutrophils, positive feedback leads to the formation of focused clusters of active Ras and PIP3, which can move as propagating waves due to negative feedback by actin (Millius *et al.*, 2009; Neilson *et al.*, 2011; Devreotes *et al.*, 2017; Gerisch *et al.*, 2019). The prevalence of interlinked positive and negative feedback loops in all of these circuits may facilitate cellular search processes in many contexts.

Undirected patch movement as a search process

How would undirected patch movement help yeast cells to mate? Mating in physiological settings may occur in crowded microcolonies, where a cell is surrounded by multiple potential mates and it might be difficult to identify a clear-cut pheromone gradient (McClure *et al.*, 2018). In similar crowded environments recreated under lab conditions, mating yeast cells frequently polarize first in the wrong direction and subsequently correct the error by moving the polarity patch into alignment with a partner (Hegemann *et al.*, 2015; Henderson *et al.*, 2019; Wang *et al.*, 2019). Thus, patch movement is required to bring partner patches into alignment.

Because secretion is directed toward the patch, the area around a moving patch becomes enriched in pheromone receptors, constituting a sensitized “nose” for pheromone (Dyer *et al.*, 2013; Hegemann *et al.*, 2015; McClure *et al.*, 2015). Moreover, each cell’s polarity patch secretes the pheromone that is detected by the partner’s “nose.” These considerations suggest that the level of pheromone sensed by partner patches that are aligned would be significantly higher than that sensed by nonaligned patches. High pheromone levels have been shown to halt patch movement (Dyer *et al.*, 2013; McClure *et al.*, 2015). Thus, an undirected search through what may be a complex and fluctuating pheromone landscape may help to bring two partner’s patches into alignment, at which point high pheromone signaling would stall patch movement, leading to mating.

Consistent with the idea that undirected patch movement is a search process, a quantitative analysis of the movement suggested that it would be effective in searching for partners. In particular, the patch movement displays angular persistence as well as a combination of small and large steps, both of which would be helpful in allowing cells to more effectively find each other.

MATERIALS AND METHODS

Live cell microscopy

Live cell microscopy was performed as described in (McClure *et al.*, 2015). Cells were grown overnight at 30°C to an OD₆₀₀ < 0.3 in Complete Synthetic Media (MP Biomedicals) supplemented with 0.67% Yeast Nitrogen Base, 2% dextrose, and 0.01% adenine. Cultures were diluted to OD₆₀₀ = 0.1–0.15 and then treated to 20 nM β-estradiol (Sigma) for 4 h. They were then mounted on a 2% agarose (Denville Scientific) slab with β-estradiol and incubated for 20 min at room temperature before imaging. Cells were imaged at 1.5-min intervals with 15 z-slices 0.5 μm apart, laser power between 10 and 15%, and 200-ms exposure on both red (561 nm) and green (488 nm) laser channels.

Analysis of patch movement

In vivo and in silico polarity patch movement were tracked in the same manner as (McClure *et al.*, 2015), where the 3D (in vivo) or 2D (in silico) centroids of polarity proteins in the patch were recorded over time. Scripts written in MATLAB 2018b (Mathworks) were used to extract and analyze step length and turning angle distributions (https://github.com/DebrajGhose/Actin_driven_patch_movement; data files, in addition to those already provided, are available on request).

Analysis of Spa2 distribution

Custom tools were developed in MATLAB 2018b to enable extraction of fluorescence intensity values along the periphery of an imaged cell (https://github.com/DebrajGhose/Actin_driven_patch_movement). A trace was drawn by hand and a three-pixel average was used to determine fluorescence intensity at each pixel along the trace. We used DLY18172 cells that were artificially arrested by

treatment with β -estradiol as described above to generate Spa2-mCherry traces along the cell periphery. Each of these traces was fit to the equation $a \times e^{-\frac{(x-u)^2}{2 \times d^2}} + c$ (a Gaussian shifted along the y-axis by c), where a , u , c and d were fit parameters and x was the distance along the cell periphery; u was used to align all the traces to the peak in order to enable averaging (Supplemental Figure S4A). The averaged trace was then fit to the equation $g \times e^{-\frac{x^2}{2 \times \sigma_a^2}} + h$, where g , h , and σ_a were fit parameters and $\sigma_a = 0.24 \mu\text{m}$ described the average width of the visible Spa2-mCherry patch (Supplemental Figure S4B).

Simulating particle movement along the surface of a sphere

Simulations and analysis were performed with MATLAB 2017b or MATLAB 2018b. To make a particle perform a random walk along the surface of a sphere, we utilized Rodrigues' rotation formula to bring it the pole, take a step (by altering the angle of elevation) in a random direction (by choosing a random azimuth), and rotated it back using Rodrigues' rotation formula. For persistent motion, we sampled the azimuth from a nonuniform distribution oriented in the direction of patch movement. Using this method allowed us to move particles along the surface of a sphere (that is, each step was a curved line); however, Figure 2B uses straight lines to indicate patch movement to make generating figures easier. The code is available at https://github.com/DebrajGhose/Actin_driven_patch_movement.

Simulating patch dynamics

Simulations and analysis were performed with MATLAB 2017b or MATLAB 2018b. For our simulations, we used a 100×100 grid to capture spatial profiles of proteins in the plasma membrane, cytosol, and the internal compartment. The reaction-diffusion equations that governed how protein concentrations changed were:

$$\frac{\partial Cdc42T}{\partial t} = (k_{2a} \cdot BemGEF + k_3 \cdot BemGEF42) \cdot Cdc42D - k_{2b} \cdot Cdc42T - k_{4a} \cdot BemGEF \cdot Cdc42T + k_{4b} \cdot BemGEF42 - k_7 \cdot BemGEFc \cdot Cdc42T + D_m \nabla^2 Cdc42T$$

$$\frac{\partial BemGEF42}{\partial t} = k_{4a} \cdot BemGEF \cdot Cdc42T - k_{4b} \cdot BemGEF42 + k_7 \cdot BemGEFc \cdot Cdc42T + D_m \nabla^2 BemGEF42$$

$$\frac{\partial BemGEF}{\partial t} = k_{1a} \cdot BemGEFc - k_{1b} \cdot BemGEF - k_{4a} \cdot BemGEF \cdot Cdc42T + k_{4b} \cdot BemGEF42 + D_m \nabla^2 BemGEF$$

$$\frac{\partial Cdc42D}{\partial t} = k_{5a} \cdot Cdc42Dc - k_{5b} \cdot Cdc42D + k_{2b} \cdot Cdc42T - (k_{2a} \cdot BemGEF + k_3 \cdot BemGEF42) \cdot Cdc42D + D_m \nabla^2 Cdc42D$$

$$\frac{\partial BemGEFc}{\partial t} = \eta \cdot (k_{1b} \cdot BemGEF - (k_{1a} + k_7 \cdot Cdc42T) \cdot BemGEFc) + D_c \nabla^2 BemGEFc$$

$$\frac{\partial Cdc42Dc}{\partial t} = \eta \cdot (k_{5b} \cdot Cdc42D - k_{5a} \cdot Cdc42Dc) + \eta \cdot (k_{5b} \cdot Cdc42Dic - k_{5a} \cdot Cdc42Dc) \cdot 0.7 + D_c \nabla^2 Cdc42Dc$$

$$\frac{\partial Cdc42Dic}{\partial t} = k_{5a} \cdot Cdc42Dc - k_{5b} \cdot Cdc42Dic + D_{ic} \nabla^2 Cdc42Dic$$

Model parameters are listed in Table 1. We used forward Euler's method with a time step of 0.05 s to simulate reaction steps and backward Euler for diffusion. Since diffusion on the membrane occurs at a slower timescale than reaction, we allowed 100 reaction steps to occur for each diffusion step to speed up simulations. We assumed components in the cytoplasm and internal compartment to be well mixed. The code is available at https://github.com/DebrajGhose/Actin_driven_patch_movement.

Yeast strains

Standard molecular biology and yeast genetics procedures were used to generate the strains used in this study (Guthrie and Fink, 1991). The strains and plasmids used in this study are listed in Table 3 and Table 4, respectively. For tracking the polarity patch, we used DLY18172 from McClure *et al.* (2015).

The alleles *rsr1::HIS3* (Schenkman *et al.*, 2002), *SPA2-mCherry:Kan^R* (Howell *et al.*, 2009), *BEM1-GFP:LEU2* (Kozubowski *et al.*, 2008), *CDC24-GFP:TRP1* (Wu *et al.*, 2015), *EXO70-GFP:Kan^R* (Moran *et al.*, 2019), *bni1::HIS3-3HA-GFP-BNI1:URA3* (Chen *et al.*, 2012), and *GFP-SEC4:URA3* (Chen *et al.*, 2012) have been described previously.

To allow artificial induction of the mating MAPK pathway, we constructed a plasmid, DLB4239, that can be used to replace the endogenous *STE5* gene, encoding the MAPK scaffold that is recruited to the plasma membrane on pheromone treatment, with two genes: 1) *GAL1pr-STE5-CTM* allows induction of a membrane-targeted Ste5 from the *GAL1* promoter and 2) *Gal4BD-hER-VP16*

Strain	Genotype
DLY18172	MATa, <i>GFP-STE4</i> , <i>GAL1pr-STE5-CTM:LEU2</i> , <i>GAL4BD-hER-VP16:TRP1</i> , <i>ste5::Nat^R</i> , <i>SPA2-mCherry:Hph^R</i> , <i>rsr1::Kan^R</i> , <i>bar1</i>
DLY23418	MATa, <i>ste5::GAL1pr-STE5-CTM:Gal4BD-hER-VP16:LEU2</i> , <i>SPA2-mCherry:Hyg^R</i> , <i>rsr1::HIS3</i> , <i>CDC24-GFP:TRP1</i>
DLY23451	MATa, <i>SPA2-mCherry:Hyg^R</i> , <i>rsr1::HIS3</i> , <i>EXO70-GFP:Kan^R</i> , <i>ste5::GAL1pr-STE5-CTM:Gal4BD-hER-VP16:LEU2</i>
DLY23421	MATa, <i>ste5::GAL1pr-STE5-CTM:Gal4BD-hER-VP16:LEU2</i> , <i>SPA2-mCherry:Hyg^R</i> , <i>rsr1::HIS3</i> , <i>GFP-linker-CDC42:URA3</i>
DLY23416	MATa, <i>ste5::GAL1pr-STE5-CTM:Gal4BD-hER-VP16:LEU2</i> , <i>SPA2-mCherry:Hyg^R</i> , <i>rsr1::HIS3</i> , <i>GFP-SEC4:URA3</i>
DLY23476	MATa, <i>SPA2-mCherry:Hyg^R</i> , <i>rsr1::HIS3</i> , <i>bni1::HIS3-3HA-GFP-BNI1:URA</i> , <i>ste5::GAL1pr-STE5-CTM:Gal4BD-hER-VP16:LEU2</i>
DLY21957	MATa, <i>ste5::GAL1pr-STE5-CTM:Gal4BD-hER-VP16:LEU2</i> , <i>SPA2-mCherry:Hyg^R</i> , <i>BEM1-GFP::LEU2</i>

TABLE 3: Strains used in this study.

Number	Genotype	Reference
DLB3102	pRS304-P(ADH1)-GAL4BD-hER-VP16	(Takahashi and Pryciak, 2008)
DLB3018	pRS305-GAL1pr-STE5-CTM	(Pryciak and Huntress, 1998)
DLB4234	pRS305-GAL1pr-STE5-CTM-ADH1pr-GAL4BD-hER-VP16	This study
DLB4239	pRS305-GAL1pr-STE5-CTM-ADH1pr-GAL4BD-hER-VP16-STE5-UTR	This study

TABLE 4: Plasmids used in this study.

expressed from the constitutive *ADH1* promoter encodes an artificial transcription factor that induces expression from the *GAL1* promoter on addition of β -estradiol to the media. In DLB4239, the two genes are flanked by 5'-UTR and 3'UTR sequences from *STE5*. Digestion with *PacI* releases a linear DNA fragment with the UTR sequences at the ends, which can replace *STE5* with the two genes by homologous recombination.

DLB4239 was constructed starting from DLB3018, which contains GAL1pr-STE5-CTM cloned into pRS305. ADH1pr-GAL4BD-hER-VP16 was amplified from DLB3102 using PCR with primers containing *NotI* sites and cloned into the *NotI* site in the DLB3018 polylinker to generate DLB4234. Overlap PCR was used to obtain a DNA fragment containing 506 base pairs upstream of the *STE5* start codon (5' UTR), a 52 base pair linker, and 457 base pairs downstream of the *STE5* stop codon (3' UTR) using yeast genomic DNA as template. This DNA fragment was inserted into the *SacI* site of DLB4234 to create DLB4239. *PacI* cuts in between the 5' and 3' UTR.

ACKNOWLEDGMENTS

We thank Timothy Elston, Samuel Ramirez, Stefano Di Talia, Jian-Geng Chiou, Katherine Jacobs, Rossie Clark-Cotton, and members of the Lew lab for reviewing the manuscript and/or stimulating discussions. We are also grateful to Patrick Ferree (for helping construct DLB4239), Yesheng Gao (for providing support with confocal imaging), Denise Ribar and Trevin Zyla (for maintaining critical lab resources), and the Duke Compute Cluster group (for providing computational resources and assistance with running simulations). This work was funded by NIH/NIGMS grant R35GM122488 to D.J.L.

REFERENCES

Adamo JE, Moskow JJ, Gladfelter AS, Viterbo D, Lew DJ, Brennwald PJ (2001). Yeast Cdc42 functions at a late step in exocytosis, specifically during polarized growth of the emerging bud. *J Cell Biol* 155, 581–592.

Artemenko Y, Lampert TJ, Devreotes PN (2014). Moving towards a paradigm: common mechanisms of chemotactic signaling in Dictyostelium and mammalian leukocytes. *Cell Mol Life Sci* 71, 3711–3747.

Ayad-Durieux Y, Knechtle P, Goff S, Dietrich F, Philippsen P (2000). A PAK-like protein kinase is required for maturation of young hyphae and septation in the filamentous ascomycete *Ashbya gossypii*. *J Cell Sci* 113 (24), 4563–4575.

Bement WM, Leda M, Moe AM, Kita AM, Larson ME, Golding AE, Pfeuti C, Su KC, Miller AL, Goryachev AB, Von Dassow G (2015). Activator-inhibitor coupling between Rho signalling and actin assembly makes the cell cortex an excitable medium. *Nat Cell Biol* 17, 1471–1483.

Bendezú FO, Martin SG (2013). Cdc42 explores the cell periphery for mate selection in fission yeast. *Curr Biol* 23, 42–47.

Bendezú FO, Vincenzetti V, Vavylonis D, Wyss R, Vogel H, Martin SG (2015). Spontaneous Cdc42 polarization independent of GDI-mediated extraction and actin-based trafficking. *PLoS Biol* 13, e1002097.

Bonazzi D, Julien JD, Romao M, Seddiki R, Piel M, Boudaoud A, Minc N (2014). Symmetry breaking in spore germination relies on an interplay between polar cap stability and spore wall mechanics. *Dev Cell* 28, 534–546.

Brandman O, Meyer T (2008). Feedback loops shape cellular signals in space and time. *Science (New York, N.Y.)* 322, 390–395.

Butty AC, Pryciak PM, Huang LS, Herskowitz I, Peter M (1998). The role of Far1p in linking the heterotrimeric G protein to polarity establishment proteins during yeast mating. *Science* 282, 1511–1516.

Castro DG, Martin SG (2018). Differential GAP requirement for Cdc42-GTP polarization during proliferation and sexual reproduction. *J Cell Biol* 217, 4215–4229.

Chen H, Kuo C-C, Kang H, Howell AS, Zyla TR, Jin M, Lew DJ (2012). Cdc42p regulation of the yeast formin Bni1p mediated by the effector Gic2p. *Mol Biol Cell* 23, 3814–3826.

Chiou J-G, Balasubramanian MK, Lew DJ (2017). Cell polarity in yeast. *Annu Rev Cell Dev Biol* 33, 77–101.

Chiou JG, Ramirez SA, Elston TC, Witelski TP, Schaeffer DG, Lew DJ (2018). Principles that govern competition or co-existence in Rho-GTPase driven polarization. *PLoS Comput Biol* 14, e1006095.

Devreotes PN, Bhattacharya S, Edwards M, Iglesias PA, Lampert T, Miao Y (2017). Excitable signal transduction networks in directed cell migration. *Annu Rev Cell Dev Biol* 33, 103–125.

Dyer JM, Savage NS, Jin M, Zyla TR, Elston TC, Lew DJ (2013). Tracking shallow chemical gradients by actin-driven wandering of the polarization site. *Curr Biol* 23, 32–41.

Etienne-Manneville S (2004). Cdc42 - the centre of polarity. *J Cell Sci* 117, 1291–1300.

Evangelista M, Blundell K, Longtine MS, Chow CJ, Adames N, Pringle JR, Peter M, Boone C (1997). Bni1p, a yeast formin linking Cdc42p and the actin cytoskeleton during polarized morphogenesis. *Science* 276, 118–122.

Garcia-Mata R, Boulter E, Burrige K (2011). The 'invisible hand': regulation of RHO GTPases by RHO GDI. *Nat Rev Mol Cell Biol* 12, 493–504.

Gerisch G, Prassler J, Butterfield N, Ecke M (2019). Actin waves and dynamic patterning of the plasma membrane. *Yale J Biol Med* 92, 397–411.

Goode BL, Eck MJ (2007). Mechanism and function of formins in the control of actin assembly. *Annu Rev Biochem* 76, 593–627.

Goryachev A, Leda M (2017). Many roads to symmetry breaking: Molecular mechanisms and theoretical models of yeast cell polarity. *Mol Biol Cell* 28, 1370–380.

Goryachev AB, Pokhilko AV (2008). Dynamics of Cdc42 network embodies a Turing-type mechanism of yeast cell polarity. *FEBS Lett* 582, 1437–1443.

Graziano BR, Weiner OD (2014). Self-organization of protrusions and polarity during eukaryotic chemotaxis. *Curr Opin Cell Biol* 30, 60–67.

Guthrie C, Fink GR (1991). Guide to yeast genetics and molecular biology. *Methods Enzymol*.

Hegemann B, Unger M, Lee SS, Stoffel-Studer I, van den Heuvel J, Pelet S, Koepl H, Peter M (2015). A cellular system for spatial signal decoding in chemical gradients. *Dev Cell* 35, 458–470.

Henderson NT, Pablo M, Ghose D, Clark-Cotton MR, Zyla TR, Nolen J, Elston TC, Lew DJ (2019). Ratiometric GPCR signaling enables directional sensing in yeast. *PLoS Biol* 17, e3000484.

Hoch HC, Staples RC, Whitehead B, Comeau J, Wolf ED (1987). Signaling for growth orientation and cell differentiation by surface topography in *Uromyces*. *Science* 235, 1659–1662.

Hong K, Nishiyama M (2010). From guidance signals to movement: signaling molecules governing growth cone turning. *Neuroscientist* 16, 65–78.

Howell AS, Savage NS, Johnson SA, Bose I, Wagner AW, Zyla TR, Nijhout HF, Reed MC, Goryachev AB, Lew DJ (2009). Singularity in polarization: rewiring yeast cells to make two buds. *Cell* 139, 731–743.

Humphries NE, Sims DW (2014). Optimal foraging strategies: Lévy walks balance searching and patch exploitation under a very broad range of conditions. *J Theor Biol* 358, 179–193.

Hwang JU, Vernoud V, Szumlanski A, Nielsen E, Yang Z (2008). A tip-localized RhoGAP controls cell polarity by globally inhibiting Rho GTPase at the cell apex. *Curr Biol* 18, 1907–1916.

- Iglesias PA, Devreotes PN (2008). Navigating through models of chemotaxis. *Curr Opin Cell Biol* 20, 35–40.
- Jilkine A, Angenent SB, Wu LF, Altschuler SJ (2011). A density-dependent switch drives stochastic clustering and polarization of signaling molecules. *PLoS Comput Biol* 7, e1002271.
- Johnson JL, Erickson JW, Cerione RA (2009). New insights into how the Rho guanine nucleotide dissociation inhibitor regulates the interaction of Cdc42 with membranes. *J Biol Chem* 284, 23860–23871.
- Johnson JM, Jin M, Lew DJ (2011). Symmetry breaking and the establishment of cell polarity in budding yeast. In: *Curr Opin Genet Dev* 21, 740–746.
- Knaus M, Pelli-Gulli MP, Van Drogen F, Springer S, Jaquenoud M, Peter M (2007). Phosphorylation of Bem2p and Bem3p may contribute to local activation of Cdc42p at bud emergence. *EMBO J* 26, 4501–4513.
- Kozubowski L, Saito K, Johnson JM, Howell AS, Zyla TR, Lew DJ (2008). Symmetry-breaking polarization driven by a Cdc42p GEF-PAK complex. *Curr Biol* 18, 1719–1726.
- Lawson MJ, Drawert B, Khammash M, Petzold L, Yi TM (2013). Spatial stochastic dynamics enable robust cell polarization. *PLoS Comput Biol* 9, e1003139.
- Layton AT, Savage NS, Howell AS, Carroll SY, Drubin DG, Lew DJ (2011). Modeling vesicle traffic reveals unexpected consequences for Cdc42p-mediated polarity establishment. *Curr Biol* 21, 184–194.
- Madden K, Snyder M (1992). Specification of sites for polarized growth in *Saccharomyces cerevisiae* and the influence of external factors on site selection. *Mol Biol Cell* 3, 1025–1035.
- Marco E, Wedlich-Soldner R, Li R, Altschuler SJ, Wu LF (2007). Endocytosis Optimizes the Dynamic Localization of Membrane Proteins that Regulate Cortical Polarity. *Cell* 129, 411–422.
- Maree AF, Grieneisen VA, Edelstein-Keshet L (2012). How cells integrate complex stimuli: the effect of feedback from phosphoinositides and cell shape on cell polarization and motility. *PLoS Comput Biol* 8, e1002402.
- McClure AW, Jacobs KC, Zyla TR, Lew DJ (2018). Mating in wild yeast: Delayed interest in sex after spore germination. *Mol Biol Cell*, mbcE18080528.
- McClure AW, Minakova M, Dyer JM, Zyla TR, Elston TC, Lew DJ (2015). Role of polarized g protein signaling in tracking pheromone gradients. *Dev Cell* 35, 471–482.
- Meinhardt H (1999). Orientation of chemotactic cells and growth cones: models and mechanisms. *J Cell Sci* 112, 2867–2874.
- Merlini L, Khalili B, Bendezú FO, Hurwitz D, Vincenzetti V, Vavylonis D, Martin SG (2016). Local pheromone release from dynamic polarity sites underlies cell-cell pairing during yeast mating. *Curr Biol* 26, 1117–1125.
- Millius A, Dandekar SN, Houk AR, Weiner OD (2009). Neutrophils establish rapid and robust WAVE complex polarity in an actin-dependent fashion. *Curr Biol* 19, 253–259.
- Moran KD, Kang H, Araujo AV, Zyla TR, Saito K, Tsygankov D, Lew DJ (2019). Cell-cycle control of cell polarity in yeast. *J Cell Biol* 218, 171–189.
- Mori Y, Jilkine A, Edelstein-Keshet L (2008). Wave-pinning and cell polarity from a bistable reaction-diffusion system. *Biophys J* 94, 3684–3697.
- Mukherjee D, Sen A, Boettner DR, Fairn GD, Schlam D, Bonilla Valentin FJ, Michael McCaffery J, Hazbun T, Staiger CJ, Grinstein S, et al. (2013). Bem3, a Cdc42 GTPase-activating protein, traffics to an intracellular compartment and recruits the secretory Rab GTPase Sec4 to endomembranes. *J Cell Sci* 126, 4560–4571.
- Nakamura M, Grebe M (2018). Outer, inner and planar polarity in the Arabidopsis root. *Curr Opin Plant Biol* 41, 46–53.
- Neilson MP, Veltman DM, van Haastert PJM, Webb SD, Mackenzie JA, Insall RH (2011). Chemotaxis: A feedback-based computational model robustly predicts multiple aspects of real cell behaviour. *PLoS Biol* 9, e1000618.
- Nern A, Arkowitz RA (1998). A GTP-exchange factor required for cell orientation. *Nature* 391, 195–198.
- Nern A, Arkowitz RA (1999). A Cdc24p-Far1p-Gβγ protein complex required for yeast orientation during mating. *J Cell Biol* 144, 1187–1202.
- Novick P, Field C, Schekman R (1980). Identification of 23 complementation groups required for post-translational events in the yeast secretory pathway. *Cell* 21, 205–215.
- Otsuji M, Ishihara S, Co C, Kaibuchi K, Mochizuki A, Kuroda S (2007). A mass conserved reaction-diffusion system captures properties of cell polarity. *PLoS Comput Biol* 3, 1040–1054.
- Ozbudak EM, Becskei A, van Oudenaarden A (2005). A system of counter-acting feedback loops regulates Cdc42p activity during spontaneous cell polarization. *Dev Cell* 9, 565–571.
- Palanivelu R, Preuss D (2000). Pollen tube targeting and axon guidance: parallels in tip growth mechanisms. *Trends Cell Biol* 10, 517–524.
- Park H-O, Bi E (2007). Central roles of small GTPases in the development of cell polarity in yeast and beyond. *Microbiol Mol Biol Rev* 71, 48–96.
- Prescianotto-Baschong C, Riezman H (1998). Morphology of the yeast endocytic pathway. *Mol Biol Cell* 9, 173–189.
- Pryciak PM, Huntress FA (1998). Membrane recruitment of the kinase cascade scaffold protein Ste5 by the Gβγ complex underlies activation of the yeast pheromone response pathway. *Genes Dev* 12, 2684–2697.
- Richman TJ, Sawyer MM, Johnson DI (2002). *Saccharomyces cerevisiae* Cdc42p localizes to cellular membranes and clusters at sites of polarized growth. *Eukaryotic Cell* 1, 458–468.
- Sartorel E, Unlu C, Jose M, Aurélie ML, Meca J, Sibarita JB, McCusker D (2018). Phosphatidylserine and GTPase activation control Cdc42 nano-clustering to counter dissipative diffusion. *Mol Biol Cell* 29, 1299–1310.
- Savage NS, Layton AT, Lew DJ (2012). Mechanistic mathematical model of polarity in yeast. *Mol Biol Cell* 23, 1998–2013.
- Schenkman LR, Caruso C, Pagé N, Pringle JR (2002). The role of cell cycle-regulated expression in the localization of spatial landmark proteins in yeast. *J Cell Biol* 156, 829–841.
- Shi C, Huang CH, Devreotes PN, Iglesias PA (2013). Interaction of motility, directional sensing, and polarity modules recreates the behaviors of chemotaxing cells. *PLoS Comput Biol* 9, e1003122.
- Slaughter BD, Unruh JR, Li R (2011). Fluorescence fluctuation spectroscopy and imaging methods for examination of dynamic protein interactions in yeast. *Methods Mol Biol* 759, 283–306.
- Strickfaden SC, Pryciak PM (2008). Distinct roles for two Galpha-Gbeta interfaces in cell polarity control by a yeast heterotrimeric G protein. *Mol Biol Cell* 19, 181–197.
- Takahashi S, Pryciak PM (2008). Membrane localization of scaffold proteins promotes graded signaling in the yeast MAP kinase cascade. *Curr Biol* 18, 1184–1191.
- Trogdon M, Drawert B, Gomez C, Banavare SP, Yi TM, Campas O, Petzold LR (2018). The effect of cell geometry on polarization in budding yeast. *PLoS Comput Biol* 14, e1006241.
- Valdez-Taubas J, Pelham HRB (2003). Slow diffusion of proteins in the yeast plasma membrane allows polarity to be maintained by endocytic cycling. *Curr Biol* 13, 1636–1640.
- Vandin G, Marenduzzo D, Goryachev AB, Orlandini E (2016). Curvature-driven positioning of Turing patterns in phase-separating curved membranes. *Soft Matter* 12, 3888–3896.
- Viswanathan GM, Raposo EP, da Luz MGE (2008). Levy flights and superdiffusion in the context of biological encounters and random searches. *Phys Life Rev* 5, 133–150.
- von Philipsborn A, Bastmeyer M (2007). Mechanisms of gradient detection: a comparison of axon pathfinding with eukaryotic cell migration. *Int Rev Cytol* 263, 1–62.
- Wang X, Tian W, Banh BT, Statler B-M, Liang J, Stone DE (2019). Mating yeast cells use an intrinsic polarity site to assemble a pheromone-gradient tracking machine. *J Cell Biol* 218, jcb.201901155.
- Watson LJ, Rossi G, Brenwald P (2014). Quantitative analysis of membrane trafficking in regulation of Cdc42 polarity. *Traffic* 15, 1330–1343.
- Wedlich-Soldner R, Altschuler S, Wu L, Li R (2003). Spontaneous cell polarization through actomyosin-based delivery of the Cdc42 GTPase. *Science* 299, 1231–1235.
- Wedlich-Soldner R, Wai SC, Schmidt T, Li R (2004). Robust cell polarity is a dynamic state established by coupling transport and GTPase signaling. *J Cell Biol* 166, 889–900.
- Woods B, Lai H, Wu CF, Zyla TR, Savage NS, Lew DJ (2016). Parallel actin-independent recycling pathways polarize Cdc42 in budding yeast. *Curr Biol* 26, 2114–2126.
- Woods B, Lew DJ (2019). Polarity establishment by Cdc42: Key roles for positive feedback and differential mobility. *Small GTPases* 10, 130–137.
- Wu C-F, Chiou J-G, Minakova M, Woods B, Tsygankov D, Zyla TR, Savage NS, Elston TC, Lew DJ (2015). Role of competition between polarity sites in establishing a unique front. *eLife* 4.
- Yu JH, Crevenna AH, Bettenbuhl M, Freisinger T, Wedlich-Soldner R (2011). Cortical actin dynamics driven by formins and myosin V. *J Cell Sci* 124, 1533–1541.